

38 Coastal ocean, Estuaries, CO₂, Carbon cycle, Air-sea CO₂ exchange, St. Lawrence Estuary, Gulf
39 of St. Lawrence, Laurentian Channel

40

41 1. Introduction

42

43 Although estuaries occupy a very small fraction (0.2 %) of the global ocean
44 surface area, their CO₂ emissions are disproportionately large compared with CO₂
45 exchanges between the open ocean and the atmosphere (Bauer et al., 2013). With an
46 estimated global efflux of 0.10–0.15 Pg C yr⁻¹ (Chen et al., 2013; Laruelle et al., 2013),
47 estuarine CO₂ degassing is thought to counterbalance CO₂ uptake on the continental
48 shelves (Chen and Borges, 2009; Laruelle et al., 2010; Cai, 2011). Almost every estuary
49 on Earth, for which data are available, is generally supersaturated with CO₂ with respect
50 to the atmosphere (Cai and Wang, 1998; Frankignoulle et al., 1998; Borges, 2005;
51 Borges et al., 2005; Borges et al., 2006; Chen and Borges, 2009; Laruelle et al., 2010;
52 Cai, 2011; Chen et al., 2012; Bauer et al., 2013; Chen et al., 2013; Regnier et al., 2013),
53 with CO₂ partial pressures (pCO₂) ranging from 400 to 10,000 µatm (in contrast, the
54 atmospheric pCO₂ in coastal zones was approximately 360–385 µatm in year 2000)
55 (Cai, 2011). Although estuaries are generally net sources of CO₂, there is considerable
56 variability and uncertainty in estimates of their CO₂ emissions, reflecting the limited
57 spatial and temporal coverage of pCO₂ measurements in estuaries as well as their
58 heterogeneous nature (hydrological and geomorphological differences, differences in
59 magnitude and stoichiometry of carbon and nutrient inputs) (Bauer et al., 2013;
60 Regnier et al., 2013).

61

62 Estuaries are geochemical reaction vessels through which continentally
63 weathered organic matter and inorganic nutrients must pass to enter the coastal ocean
64 (Kaul and Froelich, 1984). Horizontal transport is controlled by a set of physical
65 attributes (tides, wind, bathymetry, basin geography, river flow) that determine the
66 estuarine filter function (Cloern, 2001). The longer the freshwater flushing (or turnover)
67 time of the estuary, the more opportunity there is for water-column biological activity,
68 benthic exchanges and particle-dissolved phase interactions to influence its
69 biogeochemistry (Statham, 2012). Dissolved inorganic carbon (DIC) enrichments and
70 pCO₂ supersaturations observed in estuaries can be mainly attributed to the *in situ*
71 microbial degradation of internally and externally supplied organic carbon and the

72 lateral transport of inorganic carbon from rivers, coastal wetlands and ground waters
73 (Bauer et al., 2013).

74

75 In strongly tidal (macrotidal) systems, long water and particle residence times
76 (on the order of weeks to months; Middelburg and Herman, 2007) allow for the
77 extensive modification and degradation of particulate organic carbon during estuarine
78 transport (Borges et al., 2006; Chen and Borges, 2009). In the absence of seasonal or
79 permanent water stratification, the decoupling between production and degradation
80 of organic matter at and below the surface, respectively, does not occur, resulting in
81 less efficient export of DIC (Borges, 2005). Strongly tidal estuaries also tend to exhibit
82 lower levels of photosynthetic activity (Monbet, 1992) and carry greater suspended
83 particulate matter loads within their high-turbidity regions (Uncles et al., 2002;
84 Middelburg and Herman, 2007) wherein suspended particles and organic-rich
85 aggregates serve as "hot spots" of microbial recycling (Statham, 2012). Field
86 measurements suggest that 10 % of the total CO₂ emissions from the inner estuary of
87 macrotidal systems is sustained by the ventilation of riverine CO₂, whereas 90 % is due
88 to local net heterotrophy (Borges et al., 2006) fueled by inputs of terrestrial and
89 riverine-algae derived (planktonic) detritus and, in populated areas, sewage (Chen and
90 Borges, 2009). In estuaries with long freshwater residence times, the riverine CO₂ will
91 be fully ventilated to the atmosphere within the estuary, and the total CO₂ emissions
92 can be attributed to net heterotrophy (Borges and Abril, 2011).

93

94 North American estuaries rank first in terms of global estuarine surface area (41
95 %) but account for the lowest numerically averaged CO₂ flux per unit area (12 %)
96 among all continents (Chen et al., 2013). These estimates are subject to large
97 uncertainties due to data paucity. A recent synthesis by Regnier et al. (2013)
98 highlighted the meagre spatial coverage of estuarine pCO₂ measurements,
99 particularly along the Canadian eastern seaboard. Ironically, the Estuary and Gulf of St.
100 Lawrence (EGSL) in eastern Canada is the largest semi-enclosed estuarine system in
101 the world, and is among the world's most intensively studied estuaries (El-Sabh and
102 Silverberg, 1990), but was left unmentioned in recent global (Cai, 2011; Chen et al.,
103 2012; Chen et al., 2013) and regional (Laruelle et al., 2015) data compilations.
104 Furthermore, previous estuarine CO₂ studies have focused on river-dominated
105 estuaries, whereas there has been limited research on CO₂ dynamics in large estuaries

106 and bays (Joesoef et al., 2015), i.e., marine-dominated systems, including the areas of
107 mixing at sea (outer estuaries or river plumes) (Borges et al., 2005). A comparative
108 study by Jiang et al. (2008) revealed large differences in CO₂ degassing between non-
109 riverine and river-dominated estuaries and, more recently, Koné et al. (2009), Maher
110 and Eyre (2012) and Cotovicz Jr. et al. (2015) reported small CO₂ uptake by strongly
111 stratified and/or marine-dominated systems. On the U.S. east coast, the ratio of non-
112 riverine (flushed by tidal action and receiving minimum freshwater inputs) to river-
113 dominated estuaries is nearly 1:1, demonstrating the geographic importance of
114 coastal estuaries/bays on the eastern seaboard of North America (Cai, 2011).

115

116 The large-scale (width often considerably greater than the internal Rossby
117 radius; Cyr et al., 2015), macrotidal (mean tidal range greater than 2-4 m; Monbet,
118 1992) St. Lawrence Estuary is an excellent analogue of marine-dominated systems.
119 Throughout its length, the full spectrum of oceanic variability can be found (Mertz and
120 Gratton, 1990). Moreover, the basin characteristics and water transport time scales of
121 the St. Lawrence Estuary provide an almost ideal natural laboratory for geochemical
122 studies. Its surface waters have a renewal time of several months while its bottom
123 waters take several years to replenish, allowing for a comparison of spatial-temporal
124 variations in physical and chemical properties (El-Sabh and Silverberg, 1990). Given its
125 bimodal bathymetry, the St. Lawrence Estuary also permits the investigation of
126 biogeochemical processes in two types of estuary: (1) the shallow, partially mixed
127 Upper Estuary where physical mixing and abiotic processes dominate, and (2) the
128 deep, stratified Lower Estuary where biological cycling and oceanic processes prevail
129 (Yeats, 1990). As yet, no systematic study of the CO₂ dynamics in the St. Lawrence has
130 been published and, hence, the present study provides the first comprehensive
131 description of its mixed-layer carbonate chemistry, including (1) a multi-year
132 compilation of springtime and summertime pCO₂ calculated from direct
133 measurements of pH and alkalinity; (2) an area-averaged estimate of the air-sea CO₂
134 gas flux; and (3) an analysis of the relative importance of thermodynamic (temperature)
135 and biological (photosynthesis, respiration) processes in controlling the spatial
136 variability of surface-water pCO₂.

137

138 **2. Materials and methods**

139

140 2.1. Study area—St. Lawrence Estuary and Gulf

141

142 The greater St. Lawrence system (Fig. 1) connects the chain of Great Lakes, the
143 second largest terrestrial freshwater reservoir in the world, to the Atlantic Ocean (Yang
144 et al., 1996). With a drainage basin of approximately 1.32 million km², the St. Lawrence
145 River channels the second largest freshwater discharge (11,900 m³ s⁻¹) on the North
146 American continent, second only to that of the Mississippi (El-Sabh and Silverberg,
147 1990). The catchment area geology is dominated by silicate rocks of the Precambrian
148 Shield and carbonates of the Paleozoic lowlands, whose components influence the
149 downstream evolution of river chemistry (Yang et al., 1996). The erosion of the
150 carbonate rocks of the drainage basin is practically constant, as the quantity of
151 bicarbonate ions carried by the river varies little from season to season (Pelletier and
152 Lebel, 1979). On a yearly basis, between 15–20 % of the outflow of dissolved inorganic
153 carbon from the St. Lawrence River into its estuary originates from the system's
154 tributaries (e.g., Ottawa River, Mascouche River) while 80–85 % is from the Great Lakes
155 (Hélie et al., 2002). The St. Lawrence Estuary (SLE) begins at the landward limit of the
156 salt water intrusion near Île d'Orléans (~5 km downstream of Québec City) and
157 stretches 400 km seaward to Pointe-des-Monts where it widens into the Gulf of St.
158 Lawrence (GSL) (El-Sabh and Silverberg, 1990), a semi-enclosed sea with an area of
159 approximately 240,000 km² (Dufour and Ouellet, 2007) connected to the Atlantic
160 Ocean through Cabot Strait and the Strait of Belle Isle (Coote and Yeats, 1979).

161

162 Traditionally, the SLE is divided into two segments based on its bathymetry and
163 hydrographical features (Ingram and El-Sabh, 1990). The Upper St. Lawrence Estuary
164 (USLE), from Île d'Orléans, where the estuarine circulation begins, to Tadoussac, near
165 the mouth of the Saguenay Fjord, covers an area of 3,470 km². It is relatively narrow (2
166 to 24 km wide) and mostly shallow (depths less than 30 m; d'Anglejan, 1990), and
167 features an uneven, fairly complex bottom topography characterized by several
168 disconnected channels and troughs separated by ridges and islands (El-Sabh and
169 Murty, 1990). Topographically modified flows give rise to very large tidal ranges and
170 currents (up to 10 m and 3 m s⁻¹, respectively; Mertz and Gratton, 1990). In this tidally
171 energetic region, wind mixing is one to two orders of magnitude smaller than tidal
172 mixing (Painchaud et al., 1995). Owing to the resuspension of bottom sediments (tide,
173 wind or wave generated) and the net non-tidal estuarine circulation (d'Anglejan and

174 Smith, 1973), a well-developed turbidity maximum stretches between Île d'Orléans
175 and Île-aux-Coudres (Painchaud and Therriault, 1989) where suspended particulate
176 matter concentrations vary from 10 to more than 200 mg l⁻¹ (Silverberg and Sundby,
177 1979). The sources of particulate organic matter (POM) in the estuary are still debated
178 (Gearing and Pocklington, 1990). Carbon isotope studies indicate that less than half of
179 the POM is derived from terrestrial sources (Pocklington and Leonard, 1979) and is
180 quite refractory to biodegradation (Lucotte et al., 1991), whereas the major contributor
181 to POM is believed to be "fresh" organic matter, i.e., living or recently living material,
182 of river-borne origin (Tan and Strain, 1983; Hélie and Hillaire-Marcel, 2006). During the
183 spring freshet in April-May, when freshwater discharge delivers 40 % of the annual
184 solid inputs to the estuary, the input of terrigenous POM is equivalent to the average
185 POM kept in suspension in the turbidity maximum (Lucotte, 1989).

186

187 The Lower St. Lawrence Estuary (LSLE) is fairly unique in that its character is more
188 oceanic than most estuaries due to its grand size in all three dimensions and
189 unimpeded connection with Labrador and Slope waters from the Atlantic Ocean (El-
190 Sabh and Silverberg, 1990). Relative to the USLE, the LSLE is much larger (9,350 km²;
191 d'Anglejan, 1990), wider (30 to 50 km) and deeper (~300 m), and displays a smoother,
192 less variable bottom topography. Tidal currents are weaker (on the order of 30 cm s⁻¹
193 or less; Mertz and Gratton, 1990) and, under these less turbulent conditions, the Lower
194 Estuary is the major sink of continental inputs to the St. Lawrence system. Most (~75 %)
195 of the terrigenous POM carried by the St. Lawrence River is deposited on the LSLE floor
196 (Lucotte et al., 1991). The dominant bathymetric feature of the LSLE is the Laurentian
197 Channel (or Trough), a deep, central, U-shaped glaciated valley that extends 1,240 km
198 from the eastern Canadian continental shelf break through the GSL and into the LSLE
199 (d'Anglejan, 1990). The termination (head) of the Laurentian Channel at an abrupt and
200 shallow sill near Tadoussac marks the region of transition between the Upper and
201 Lower Estuary and is an area of complex tidal phenomena (Gratton et al., 1988). Due
202 to rapid shoaling, tidal movements (e.g., internal tides and strong flows over the steep
203 sill) locally generate significant mixing of surface freshwater with cold, nutrient-rich
204 waters from the intermediate and deep layers of the Gulf, resulting in a fertile surface
205 layer that flows continuously seaward (Coote and Yeats, 1979; Saucier and Chassé,
206 2000) and sustains important feeding habitats for several large marine mammals
207 (Dufour and Ouellet, 2007). The Lower Estuary's seaward outflow, together with the

208 Gaspé Current, a rapidly moving coastal jet, are a major input of nutrients and
209 zooplankton to the near-surface waters of the GSL (Coote and Yeats, 1979; Plourde
210 and Runge, 1993). Mesoscale features such as coastal jets, internal Kelvin waves,
211 baroclinic eddies and unstable waves are all possible due to strong Coriolis effects
212 (Ingram and El-Sabh, 1990).

213

214 The Lower St. Lawrence Estuary is one of the most laterally stratified estuaries in
215 the world (Larouche et al., 1987), and is also strongly vertically stratified. During
216 summertime, the SLE can be described as a three-layer system on the basis of its
217 thermal stratification (Gratton et al., 1988). Each spring, a new surface layer flow is
218 initiated by the freshwater runoff from the St. Lawrence River, Saguenay Fjord and
219 rivers on the north shore of the estuary (Dufour and Ouellet, 2007; see Fig. 1).
220 Discharge from the St. Lawrence River (mean annual discharge of $10,000 \text{ m}^3 \text{ s}^{-1}$,
221 peaking at $15,000 \text{ m}^3 \text{ s}^{-1}$ during the spring freshet; Painchaud and Therriault, 1989)
222 provides about 80 % of the total freshwater input to the estuary (Ingram and El-Sabh,
223 1990), whereas the combined runoff from the Saguenay and Manicouagan Rivers
224 accounts for most of the remainder (Tee, 1990). The warm and relatively fresh surface
225 layer (0 to 30 m) overlies the cold intermediate layer or CIL (30–150 m deep; $S_p = 32.0$
226 to 32.6) that is formed by advection of the Gulf's wintertime surface mixed layer
227 (Galbraith, 2006). Below the CIL, a warmer (2 to 6 °C) and saltier ($S_p = 33$ to 35) bottom
228 layer (>150 m deep), originating from the mixing of western-central Atlantic and
229 Labrador shelf waters that intrude at depth primarily through Cabot Strait, flows
230 sluggishly landward ($\sim 0.5 \text{ cm s}^{-1}$; Bugden, 1988) toward the head region of the
231 Laurentian Channel (Saucier et al., 2003; Gilbert et al., 2005).

232

233 **2.2. Water-column sampling and analytical procedures**

234

235 Water samples were collected aboard the RV *Coriolis II* during ten research
236 cruises within the St. Lawrence Estuary and Gulf in the ice-free spring or summer season
237 between 2003 and 2016. Water sampling was conducted mainly along the central axis
238 of the St. Lawrence Estuary and the Laurentian Channel. The sampling locations are
239 shown in Fig. 2. Samples were taken from discrete depths throughout the water
240 column, typically at 3 m, 20 m, 50 m, 70 m, 100 m and at 50m intervals to the bottom
241 (or within 10 m of the bottom). A comprehensive dataset was compiled from field or

242 laboratory measurements of the following physical–chemical properties: temperature
243 (T), practical salinity (S_P), pH_{NBS} and/or pH_T , total alkalinity (TAlk), dissolved inorganic
244 carbon (DIC), soluble reactive phosphate (SRP), and dissolved silicate (DSi), nitrate
245 (NO_3) and oxygen (DO).

246

247 T and S_P were determined *in situ* using the conductivity-temperature-depth
248 (CTD) probe (SeaBird SBE 911) mounted on the sampling rosette. The temperature
249 probe was calibrated by the manufacturer, whereas the conductivity sensor was
250 calibrated by the manufacturer and recalibrated using discrete salinity samples
251 collected throughout the water column and analyzed on a Guildline Autosol 8400
252 salinometer calibrated with IAPSO standard seawater. Water samples destined for pH
253 and TAlk measurements were transferred directly from the 12L Niskin bottles mounted
254 on the CTD-rosette system to, respectively, 125mL plastic bottles without headspace
255 and 250mL glass bottles as soon as the rosette was secured onboard. In the latter case,
256 a few crystals of $HgCl_2$ were added before the bottle was sealed with a ground-glass
257 stopper and Apiezon® Type-M high-vacuum grease.

258

259 pH was determined onboard at 25 °C, potentiometrically on the NBS/NIST scale
260 (infinite dilution convention, pH_{NBS}) for low salinity waters ($S_P < 5$) and
261 potentiometrically and/or colorimetrically on the total hydrogen ion concentration
262 scale (constant ionic medium convention, pH_T) for higher salinity waters.
263 Potentiometric pH measurements were carried out using a Radiometer Analytical®
264 GK2401C combination glass electrode connected to a Radiometer Analytical® PHM84
265 pH/millivolt-meter. Prior to each measurement, the electrode was calibrated against
266 three NIST-traceable buffer solutions: pH-4.00, pH-7.00 and pH-10.00 at 25°C. The
267 electrode response to these buffers was then least-squares fitted to obtain the
268 Nernstian slope. For $S_P > 5$, pH measurements were converted to the pH_T scale using
269 TRIS buffer solutions prepared at $S_P = 5, 15, 25, \text{ or } 35$ for which the pH_T was assigned
270 at 25°C (Millero, 1986). Colorimetric pH measurements were carried out using a
271 Hewlett-Packard UV-Visible diode array spectrophotometer (HP-8453A) and a 5cm
272 quartz cell after thermal equilibration of the plastic sampling bottles in a constant
273 temperature bath at $25.0 \pm 0.1^\circ C$. Phenol red (Robert-Baldo et al., 1985) and *m*-cresol
274 purple (Clayton and Byrne, 1993) were used as color indicators. The pH_T of the water

275 samples and buffer solutions were calculated according to the equation of Byrne
276 (1987). The reproducibility of the pH measurements was typically better than ± 0.003 .
277

278 TAlk was measured at McGill University using an automated Radiometer
279 (TitraLab865®) potentiometric titrator and a Red Rod® combination pH electrode
280 (pHC2001). The dilute HCl titrant was calibrated prior, during, and after each titration
281 session using certified reference materials provided by Andrew Dickson (Scripps
282 Institute of Oceanography). Raw titration data were processed with a proprietary
283 algorithm specifically designed for shallow end-point detection. The reproducibility of
284 the method was better than 0.5 %.

285

286 Direct DIC measurements were carried out during an additional cruise in 2014
287 using a Scitech Apollo DIC analyzer. After being thermostated at 25 °C, 1-1.5 mL of the
288 sample was injected into the instrument's reactor where it was acidified with 10 %
289 H₃PO₄ and the evolved CO₂ carried by a stream of pure nitrogen to a LICOR infrared
290 analyzer. A calibration curve was constructed using gravimetrically-prepared Na₂CO₃
291 solutions, and the accuracy of the measurements was verified using certified reference
292 material solutions provided by Andrew Dickson (Scripps Institute of Oceanography).
293 The reproducibility of the measurements was typically on the order of 0.2 %. Results of
294 the direct DIC measurements were used to assess the contribution of organic alkalinity
295 to the total alkalinity in the Upper Estuary, as discussed in Section 2.3.2.

296

297 DO concentrations were determined by Winkler titration (Grasshoff et al., 1999)
298 on distinct water samples recovered directly from the Niskin bottles. The relative
299 standard deviation, based on replicate analyses of samples recovered from the same
300 Niskin bottle, was better than 1 %. These measurements further served to calibrate the
301 SBE-43 oxygen probe mounted on the rosette. For the determination of nutrient
302 concentrations, aliquots of the water samples taken from the Niskin bottles were
303 syringe filtered through a 0.45µm Millipore polycarbonate (MA) filter. DSi was
304 measured onboard on the same day of sampling using the method described in
305 Grasshoff et al. (1999). Water samples destined for NO₃ and SRP measurements were
306 transferred, respectively, into acid-washed 15ml polyethylene and borosilicate tubes,
307 quickly frozen and stored at -20 °C. Their concentrations were determined using
308 standard colorimetric methods adapted from Grasshoff et al. (1999) with a SEAL

309 Autoanalyzer III at the Institut des Sciences de la Mer de Rimouski. The analytical
310 detection limit was 0.04 μM for NO_3 , 0.05 μM for SRP and 0.1 μM for DSi. Based on
311 replicate analyses of the standards, the reproducibility of these measurements was
312 typically 1 %.

313

314 The *in situ* pressure and density of the samples were calculated from the
315 Thermodynamic Equation of Seawater - 2010 (TEOS-10) using the Gibbs Seawater
316 (GSW) Oceanographic Toolbox (MATLAB-version 3.05; McDougall and Barker, 2011).
317 All field measurements reported in $\mu\text{mol L}^{-1}$ were converted to $\mu\text{mol kg}^{-1}$ using the *in*
318 *situ* density data.

319

320 **2.3. Calculation of aqueous pCO_2**

321

322 **2.3.1. pCO_2 in mixed-layer waters**

323

324 Aqueous pCO_2 ($\text{pCO}_2(\text{water})$) is defined as the partial pressure of carbon
325 dioxide in wet (100 % water-saturated) air that is in equilibrium with the water sample.
326 Because direct pCO_2 measurements were not available from the RV *Coriolis II* cruises,
327 $\text{pCO}_2(\text{water})$ (μatm) and DIC ($\mu\text{mol kg}^{-1}$) were calculated from the measured pH (total
328 or NBS scale) and TAlk ($\mu\text{mol kg}^{-1}$), at *in situ* temperature ($^{\circ}\text{C}$), salinity (S_P) and pressure
329 (dbar), using the program CO2SYS (MATLAB-version 1.1; van Heuven et al., 2011) and
330 the carbonic acid dissociation constants (K_1 , K_2) of Cai and Wang (1998) for estuarine
331 waters. Wherever data were available, the contributions to TAlk from phosphate and
332 silicate were included in the calculations. Although the K_1 and K_2 formulations from
333 Lueker et al. (2000) are recommended for best practices by Dickson et al. (2007), they
334 are not suitable for the low-salinity conditions found in estuaries ($S_P < 19$) (Orr et al.,
335 2015). The revised equations for K_1 and K_2 from Cai and Wang (1998) are applicable
336 over a larger range of salinities (0 to 40) and, thus, were used to examine the carbonate
337 system in the estuarine waters of our study area.

338

339 This study focuses on the CO_2 dynamics in near-surface waters. To obtain
340 individual data points of surface-water pCO_2 at each sampling location, the pCO_2 data
341 in the surface mixed layer (SML) were averaged. The SML is the site of active air-sea
342 interaction where heat and gases are exchanged directly with the atmosphere and

343 within which physical (temperature, salinity, density) and chemical (dissolved gases)
344 properties are vertically homogeneous due to turbulent mixing (Sprintall and Tomczak,
345 1992). The lower limit to air-sea interaction, i.e., the mixed layer depth (MLD), is
346 demarcated by a pycnocline, a sharp density gradient that generally coincides with
347 both a temperature (thermocline) and salinity (halocline) gradient. Here, we determine
348 the thickness of the SML using a density-based criterion which defines the MLD as the
349 depth at which a threshold difference of 0.03 kg m^{-3} from the sea surface occurs (de
350 Boyer Montégut et al., 2004). In the following sections, surface-water pCO_2 will be
351 taken to mean the SML-averaged pCO_2 .

352

353 **2.3.2. Sources of error in pCO_2 calculation**

354

355 In this study, pH/Talk was used as the input combination to study the
356 consistency between calculations of pCO_2 using different sets of carbonic acid
357 dissociation constants. The importance of using appropriate formulations of K_1 and K_2
358 in estuarine waters is shown by the discrepancies in the calculated pCO_2 values (pCO_2
359 @ 15°C) at low salinities (Fig. 3). The percent difference between values calculated
360 using the dissociation constants of Cai and Wang (1998) and those calculated using
361 the best-practices constants of Lueker et al. (2000) was on average 3.07 %. At $S_P < 19$,
362 differences between the calculated pCO_2 values were as large as 18.0 % (average
363 difference of 6.88 %), whereas, at $S_P > 19$, the calculated values were in better
364 agreement (only ~ 1.48 % difference). The K_1 and K_2 formulations of Millero (2010), the
365 most recent set of constants proposed for estuarine waters ($S_P = 1$ to 50), yielded pCO_2
366 values that differed substantially from those derived using the constants of Cai and
367 Wang (1998) at $S_P < 19$, with the largest divergence reaching 34.4 % (average
368 difference of 13.6 %). At $S_P = 0$, the pCO_2 values calculated using the constants of Cai
369 and Wang (1998) compared very well with those given by the Millero (1979) constants
370 for freshwater (difference of only ~ 0.08 %), whereas the pCO_2 values calculated using
371 the constants of Millero (2010) showed very poor agreement with the freshwater results
372 (differing by ~ 34.3 %). These discrepancies highlight the need for new or revised
373 measurements of the carbonic acid dissociation constants under estuarine conditions
374 (in brackish waters) especially at $S_P < 5$. Studies which use the best-practices
375 formulations of K_1 and K_2 to calculate estuarine pCO_2 may underestimate CO_2

376 emissions at low salinities, whereas those that implement the Millero (2010)
377 formulations may produce overestimates.

378

379 Another potential source of error in the calculation of $p\text{CO}_2$ (pH/TAlk) in low-
380 salinity estuarine waters is the contribution of dissolved organic compounds to the total
381 alkalinity. The contributions of borate, phosphate and silicate species are taken into
382 consideration in CO2SYS, whereas the magnitude of organic alkalinity (Org-Alk, or
383 excess alkalinity) is usually assumed to be small or negligible, and is simply ignored
384 when using TAlk to calculate $p\text{CO}_2$ in open ocean waters. In riverine and coastal waters,
385 however, the contribution of organic species to the TAlk can be significant (Yang et al.,
386 2015). Rivers draining organic-rich soils and non-carbonate rocks have low DIC
387 concentrations (a few hundred $\mu\text{mol L}^{-1}$) that are often exceeded by dissolved organic
388 carbon (DOC) concentrations (Abril et al., 2015). As discussed by Hunt et al. (2011), a
389 significant contribution of Org-Alk (the organic acid anions in DOC) leads to an
390 overestimation of calculated $p\text{CO}_2$ using any algorithm that accounts only for the
391 contributions of inorganic species to TAlk. A comparison of the calculated TAlk
392 (DIC/pH) and the measured TAlk from the 2014 cruise reveals that Org-Alk is on the
393 order of $-20 \mu\text{mol kg}^{-1}$ for the St. Lawrence River end-member, whereas it is as high as
394 $-120 \mu\text{mol kg}^{-1}$ for the Saguenay River end-member (A. Mucci, pers. comm.). Given that
395 TAlk exceeds $\sim 1000 \mu\text{mol kg}^{-1}$ throughout our study area and the Saguenay River
396 contribution to the surface waters of the SLE is limited (at most $\sim 6\%$ at the head of the
397 Lower Estuary; Mucci et al., in revision), consideration of the Org-Alk in the calculation
398 of $p\text{CO}_2$ (pH/TAlk) yielded values that were at most 1.9% different from those
399 uncorrected for Org-Alk. Bearing in mind the uncertainties in the K_1 and K_2
400 formulations as well as the analytical uncertainties, the influence of Org-Alk on the
401 calculated $p\text{CO}_2$ (pH/TAlk) did not represent a significant source of error.

402

403 **2.4. Temperature normalization of $p\text{CO}_2$**

404

405 The effect of temperature on aqueous $p\text{CO}_2$ is primarily the manifestation of
406 changes in the solubility of CO_2 gas in water (Takahashi et al., 1993). The temperature
407 dependence of $p\text{CO}_2$ in seawater, i.e., $\partial \ln(p\text{CO}_2) / \partial T = 0.0423 \text{ }^\circ\text{C}^{-1}$, was determined
408 experimentally by Takahashi et al. (1993) on a single North Atlantic surface water
409 sample with $S_p = 35.380$ under isochemical conditions. As this oft-used approximation

410 for thermally induced changes in pCO₂ was derived from direct measurements in open
411 ocean waters, we use a different approach to remove the temperature effect on the
412 estuarine pCO₂ in our study area. The *in situ* pCO₂ were normalized to the average
413 surface-water temperature (pCO₂(\overline{SST}), $\overline{SST} = 7.82$ °C), using the temperature
414 normalization method of Jiang et al. (2008) in which pCO₂ values are re-calculated from
415 the TAlk and DIC data at a common temperature. The results yielded a temperature
416 coefficient of $\partial \ln(pCO_2) / \partial T = 0.0402$ °C⁻¹ (R²= 0.99), in excellent agreement with that
417 of Takahashi et al. (1993). The pCO₂ changes due to temperature deviations from \overline{SST}
418 ($\Delta pCO_2(temp)$) were calculated as:

$$419 \Delta pCO_2(temp) = pCO_2(obs) - pCO_2(\overline{SST}) \quad (1)$$

421
422 where pCO₂(obs) is the *in situ* pCO₂ and pCO₂(\overline{SST}) is the temperature-normalized
423 pCO₂. Since changes in pCO₂ at a common temperature primarily reflect changes in
424 DIC, the spatial variations in pCO₂(\overline{SST}) can be attributed to the combined influences
425 of non-thermal processes that affect DIC (water mass mixing, biological activity).
426 Theoretically, pCO₂(\overline{SST}) can be further partitioned into the pCO₂ change due to
427 biology and that due to mixing through an analysis of the water mass structure, e.g., an
428 optimum multiparameter (OMP) water mass analysis. Results from its application will
429 be presented in a subsequent study.

430

431 2.5. Air-sea CO₂ flux estimation

432

433 Air-sea CO₂ gas exchange (F, mmol C m⁻² d⁻¹) at each sampling location was
434 estimated as follows:

435

$$436 F = k \cdot K_0 \cdot (pCO_2(water) - pCO_2(air)) \quad (2)$$

437

438 where k (cm h⁻¹) is the gas transfer velocity of CO₂, K₀ (mol kg⁻¹ atm⁻¹) is the solubility
439 coefficient of CO₂ at *in situ* surface-water temperature and salinity (Weiss, 1974), and
440 pCO₂(water) and pCO₂(air) (μatm) are the partial pressures of CO₂ in the water and the
441 air, respectively. The difference between pCO₂(water) and pCO₂(air) (ΔpCO_2)
442 determines the direction of gas exchange across the air-sea interface. Positive values
443 of F indicate CO₂ release by the surface water, whereas negative values indicate CO₂

444 uptake. Conversion factors were applied to express the final F with the aforementioned
445 units.

446

447 Atmospheric pCO_2 ($pCO_2(\text{air})$) was calculated using the monthly averages of the
448 measured mole fraction of CO_2 in dry air (xCO_2 , at the greenhouse gas observational
449 station in Fraserdale, Ontario) obtained from the Climate Research Division at
450 Environment and Climate Change Canada. The mean $pCO_2(\text{air})$ in the sampling month
451 was computed using the relationship (Takahashi et al., 2002):

452

$$453 \quad pCO_2(\text{air}) = xCO_2 \cdot (P_b - P_w) \quad (3)$$

454

455 where xCO_2 is in ppm, P_b (atm) is the atmospheric (or barometric) pressure at the sea
456 surface, and P_w (atm) is the equilibrium (or saturation) water vapor pressure at *in situ*
457 surface-water temperature and salinity (Weiss and Price, 1980). One-month averaged
458 barometric pressures were calculated using the hourly station pressure data from
459 Environment Canada at the following weather observing stations: Québec/Jean
460 Lesage International Airport (Upper Estuary), Mont-Joli Airport (Lower Estuary), and
461 Gaspé Airport (Gulf of St. Lawrence). The P_b at station elevation was converted to mean
462 sea level pressure using the formula of Tim Brice and Todd Hall (NOAA's National
463 Weather Service, http://www.weather.gov/epz/wxcalc_stationpressure).

464

465 The formulation of the gas transfer velocity, k , is the largest source of error in the
466 computation of air-sea CO_2 fluxes (Borges et al., 2004a,b). Properly constraining values
467 of k in estuaries is problematic (Raymond and Cole, 2001) due to their hydrodynamic
468 and geomorphologic complexity (Abril et al., 2000). Gas transfer is thought to be
469 regulated by turbulence at the air-water interface (Wanninkhof, 1992). Wind stress
470 plays a key role in the generation of turbulence at the ocean surface through the
471 transfer of momentum to waves and currents (Ho et al., 2011), whereas, in estuarine
472 environments and especially macrotidal estuaries, surface turbulence can be created
473 by interactions of wind forcing, tidal currents and boundary friction (Zappa et al., 2003,
474 Borges et al., 2004a,b; Zappa et al., 2007) and, in turbid estuaries, attenuated by
475 suspended material (Abril et al., 2009). The turbulence generated from bottom stress
476 varies with water depth and tidal velocity (Raymond et al., 2000), and is important only
477 in shallower estuaries with high current velocities (Cerco, 1989). Raymond and Cole

478 (2001) have shown that wind stress controls turbulence at the air-water interface for all
479 systems with depths greater than 10 meters (at depths < 10 m, either wind or bottom
480 stress may dominate).

481

482 Several different predictive relationships between wind speed and gas transfer
483 velocity have been proposed based on laboratory and field studies. Here, we estimate
484 the latter from short-term (or steady) wind speed measurements using the equations
485 of Wanninkhof (1992) revised by Wanninkhof (2014) and Raymond and Cole (2001):

486

487 k from Wanninkhof (2014), denoted as k_{W-14} :

$$488 \quad k_{W-14} = 0.251 u^2 (Sc / 660)^{-0.5} \quad (4)$$

489

490 k from Raymond and Cole (2001), denoted as $k_{R\&C-01}$:

$$491 \quad k_{R\&C-01} = 1.91 e^{0.35u} (Sc / 660)^{-0.5} \quad (5)$$

492

493 where u is the wind speed ($m s^{-1}$) and Sc is the Schmidt number ($Sc = \mu/D$, where μ is
494 the kinematic viscosity of the water and D is the diffusion coefficient) for CO_2 gas in
495 solution. The Schmidt number for CO_2 in seawater at $20^\circ C$ is 660 and was adjusted to
496 $Sc=600$ for freshwater. Hourly wind speed data were obtained from Environment
497 Canada at the aforementioned weather observing stations, and averaged over the
498 sampling month to obtain short-term wind speeds. The correction to a common
499 Schmidt number was performed using the equations of Wanninkhof (1992) for the
500 temperature dependence of Sc for CO_2 gas in seawater ($S_P=35$) and freshwater,
501 respectively, and assuming that k is proportional to $Sc^{-0.5}$.

502

503 Because of increased turbulence, one would expect k values calculated from
504 estuarine parameterizations to be higher than those predicted from oceanic
505 parameterizations at equivalent wind speeds (Abril et al., 2000). Within the confines of
506 the SLE, estimates of k using the Wanninkhof (2014) relationship ranged from 1.6 to
507 $4.5 cm h^{-1}$ whereas those calculated from Raymond and Cole (2001) were between 3.8
508 and $8.1 cm h^{-1}$. Hence, we take the air-sea CO_2 flux values calculated with k_{W-14} to be
509 the theoretical lower limit of gas exchange (F_{W-14}), whereas those computed from $k_{R\&C-01}$
510 represent the upper limit of gas exchange ($F_{R\&C-01}$).

511

512 In order to estimate the area-averaged CO₂ flux in the SLE, the estuary proper
513 was divided into five segments, with each section containing at least one sampling
514 location. Given that the Lower Estuary occupies ~75 % of the total estuarine surface
515 area, and encompasses a fairly wide range of pCO₂ values (standard deviation of 119
516 μatm), the SLE was divided into longitudinal sections (Fig. 2) rather than segmented by
517 salinity. The fluxes in each segment were normalized to the sectional surface area and
518 then summed to obtain a spatially integrated air-sea CO₂ flux ($F_{area-avg}$) for the whole
519 estuary, as follows (Jiang et al., 2008):

520

$$521 \quad F_{area-avg} = \frac{\sum F_i S_i}{\sum S_i} \quad (6)$$

522

523 where F_i is the average of all the fluxes within segment i , and S_i is the surface area of
524 segment i . Sectional surface areas were tabulated in MATLAB using the land mask of
525 eastern Canada obtained from Fisheries and Oceans Canada. An area-averaged CO₂
526 flux was obtained for both the upper and lower limits of gas exchange in the SLE. These
527 two final estimates are assumed to bracket the real areal CO₂ flux.

528

529 **2.6. Conceptual framework for the analysis of variations in biogenic gas** 530 **concentrations**

531

532 A comparison of the distribution of biologically reactive dissolved gases, i.e.,
533 CO₂ and O₂, can provide useful information about the physical (thermal) and biological
534 processes controlling their concentrations (Richey et al., 1988). Temperature-related
535 gas solubility effects occur in the same direction for CO₂ and O₂, whereas biological
536 production and respiration affect CO₂ and O₂ in opposite directions. Following the
537 approach of Carrillo et al. (2004), the saturation states (or % saturation) of pCO₂ and
538 DO, with respect to the atmosphere, were compared in order to determine the relative
539 importance of temperature effects (heating or cooling) and biological activity
540 (photosynthesis or respiration) in the surface waters at each sampling location. The
541 pCO₂ percent saturation (pCO₂(% sat)) was calculated as follows:

542

$$543 \quad pCO_2(\% \text{ sat}) = (pCO_2(\text{water}) / pCO_2(\text{air})) \cdot 100 \quad (7)$$

544

545 The DO percent saturation (DO(% sat)) was calculated as:

546

$$547 \quad DO(\% \text{ sat}) = (DO/DO^*) \cdot 100 \quad (8)$$

548

549 where DO^* is the equilibrium DO concentration ($\mu\text{mol kg}^{-1}$) at *in situ* surface-water
550 temperature and salinity (Benson and Krause, 1984). The relationship between DO(%
551 sat) and $p\text{CO}_2$ (% sat) is roughly analogous to that of the apparent oxygen utilization
552 (AOU) and excess DIC (eDIC) (Abril et al., 2000). The former is defined as the difference
553 between DO^* and DO, whereas the latter is defined as the difference between the
554 observed DIC and a theoretical DIC at atmospheric equilibrium.

555

556 According to the method of Carrillo et al. (2004), data points fall into one of four
557 quadrants on a graph of DO(% sat) versus $p\text{CO}_2$ (% sat), with the origin at 100 %
558 saturation for both gases. Quadrant I (upper left; supersaturated DO, undersaturated
559 $p\text{CO}_2$) suggests net photosynthesis, Quadrant II (upper right; supersaturated DO and
560 $p\text{CO}_2$) indicates the effects of heating, Quadrant III (lower right; undersaturated DO,
561 supersaturated $p\text{CO}_2$) implies net respiration, and Quadrant IV (lower left;
562 undersaturated DO and $p\text{CO}_2$) represents the effects of cooling. Although general
563 patterns become apparent, we urge caution in the interpretation of these results as
564 significant limitations apply. Surface-water CO_2 and O_2 may be acted upon by other
565 forcings such as air-sea gas exchange. The net transfer of CO_2 and O_2 gases occurs
566 across the air-sea interface whenever their partial pressures in the SML differ from those
567 in the atmosphere. Because of their differential gas exchange rates (i.e., O_2 exchanges
568 ~ 19 times faster than CO_2 ; Peng et al., 1987), CO_2 and O_2 dynamics may be decoupled
569 in surface waters, causing an asymmetry in the observed CO_2 : O_2 relationship (Carrillo
570 et al., 2004).

571

572 **3. Results and discussion**

573

574 **3.1. Spatial variability of surface-water $p\text{CO}_2$**

575

576 Data were compiled from all ten cruises to describe the inorganic carbon
577 chemistry in the mixed-layer waters of the St. Lawrence River, Upper Estuary, Lower
578 Estuary and Gulf (Table 1). Large spatial variations in surface-water $p\text{CO}_2$ were
579 observed within the EGSL system, with values ranging from 139 to 765 μatm (452 ± 134

580 μatm) during the spring/summer sampling periods. Overall, the pCO_2 were higher in
581 the USLE ($571 \pm 72 \mu\text{atm}$) than in the LSLE ($394 \pm 119 \mu\text{atm}$) and GSL ($352 \pm 80 \mu\text{atm}$),
582 whereas the atmospheric pCO_2 showed less variability, ranging from 372 to 405 μatm ,
583 during the sampling years. As shown in Fig. 4, the USLE was always a CO_2 source (i.e.,
584 surface-water pCO_2 were above atmospheric level) while the LSLE and GSL were
585 generally either a CO_2 sink or nearly neutral (i.e., surface-water pCO_2 were below or
586 close to atmospheric level).

587

588 Within the confines of the SLE, the surface-water pCO_2 generally decreased with
589 increasing distance from the head of the estuary (Île d'Orléans) and along the salinity
590 gradient (Fig. 4 and 5). The highest values of pCO_2 were observed near the landward
591 limit of the salt water intrusion in the SLE's upper reaches, in the vicinity of the Cap
592 Tourmente intertidal flats and marshes. This area ($3 \times 10^6 \text{ m}^2$) is located along the core
593 of the estuary's maximum turbidity zone (MTZ) (Lucotte and d'Anglejan, 1986). The
594 lowest surface-water pCO_2 were found downstream of the MTZ in the lower reaches of
595 the SLE near Pointe-des-Monts, where the channel widens into the gulf. Due to
596 favorable environmental conditions (nutrients, light, stratification), phytoplankton
597 blooms typically occur in late spring or early summer in the LSLE (Zakardjian et al.,
598 2000), with maximal biological production occurring in its downstream portion due to
599 the mixing of cold, nutrient-rich waters, upwelled at the head of the Laurentian
600 Channel, with warmer freshwaters flowing in from the north shore rivers (Savenkoff et
601 al., 1994). Seaward from the estuary-gulf boundary, the pCO_2 gradually increased from
602 207 to 478 μatm , coinciding with rising surface-water temperatures ($T = 3.9$ to $13.7 \text{ }^\circ\text{C}$).

603

604 The spatial variability of surface-water pCO_2 due to temperature variations was
605 removed by normalizing the pCO_2 data to a common temperature ($T = 7.82 \text{ }^\circ\text{C}$). From
606 a comparison of the *in situ* and corresponding temperature-normalized pCO_2 , spatial
607 variations in surface-water temperature lowered or raised the pCO_2 by -122 to 181
608 μatm within the EGSL system. The maximum (minimum) values of $\Delta\text{pCO}_2(\text{temp})$,
609 expressed as a percent change, were 38 % (-14 %) in the USLE, 24 % (-20 %) in the
610 LSLE, and 29 % (-17 %) in the GSL. Temperature normalization, however, removed only
611 a small part of the overall spatial variability of surface-water pCO_2 (Fig. 6). Given that
612 the spread of the $\text{pCO}_2(\overline{\text{SST}})$ data remained large (153-668 μatm ; $447 \pm 133 \mu\text{atm}$),

613 most of the spatial variability in surface-water pCO₂ can be explained by non-thermal
614 physical and biological processes that affect DIC concentrations in the mixed layer.

615

616 **3.2. Air-sea CO₂ flux and spatial integration**

617

618 Large spatial variations in the air-sea CO₂ flux were observed within the EGSL
619 system during the spring/summer sampling months, with fluxes ranging from -21.9 to
620 28.4 mmol m⁻² d⁻¹ (Fig. 7). Values of F were always positive in the USLE (2.0 to 28.4
621 mmol m⁻² d⁻¹) and either negative or positive in the LSLE (-21.9 to 15.1 mmol m⁻² d⁻¹)
622 and GSL (-8.4 to 3.6 mmol m⁻² d⁻¹). As expected, F_{R&C-01} (estuarine parameterization of
623 k) were larger than F_{W-14} (oceanic parameterization of k) due to the inherently greater
624 surface turbulence in estuarine systems. The average difference between CO₂ fluxes
625 calculated using the two formulations of the gas transfer velocity (equations 4 and 5)
626 was 71.7 %. Details of the k and F values given by each parameterization of k are shown
627 in Table 2. Irrespective of the parameterization, the calculated CO₂ fluxes were more
628 positive in the USLE (9.2 ± 5.3 mmol m⁻² d⁻¹) than in the LSLE (0.8 ± 7.2 mmol m⁻² d⁻¹)
629 and GSL (-1.2 ± 3.0 mmol m⁻² d⁻¹).

630

631 The SLE was divided into five segments to obtain an area-averaged CO₂ flux for
632 the whole estuary. The data used to calculate the F_{area-avg} are listed in Table 3. Overall,
633 the SLE served as a weak source of CO₂ to the atmosphere at the time of sampling,
634 with an area-averaged degassing flux of 0.98 to 2.02 mmol C m⁻² d⁻¹ (0.36 to 0.74 mol
635 C m⁻² yr⁻¹) during the late spring and early summer. This efflux compares favorably with
636 that of the Delaware Estuary (2.4 ± 4.8 mol C m⁻² yr⁻¹; Joesoef et al., 2015), another
637 large estuarine system with a long water residence time, but is significantly lower than
638 estimates in the marine-dominated Sapelo and Dobby Sound estuaries (10.5 to 10.7
639 mol C m⁻² yr⁻¹; Jiang et al., 2008). From a compilation of 165 estuaries worldwide,
640 almost all systems, with the exception of those in the Arctic (-1.1 mol C m⁻² yr⁻¹), serve
641 as sources of CO₂ to the atmosphere (Chen et al., 2013). Chen et al. (2013) concluded
642 that the world's upper estuaries (S_p < 2) are strong sources (39.0 ± 55.7 mol C m⁻² yr⁻¹),
643 mid estuaries (2 < S_p < 25) are moderate sources (17.5 ± 34.2 mol C m⁻² yr⁻¹), and lower
644 estuaries (S_p > 25) are weak sources (8.4 ± 14.3 mol C m⁻² yr⁻¹). Predictably, with its
645 maritime region occupying almost three-fourths of the total surface area, the SLE
646 behaves like an outer estuary with only small CO₂ evasion. The lack of temporal

647 coverage of surface-water pCO₂ data, however, prevents us from reliably synthesizing
648 an annual air-sea CO₂ flux.

649

650 **3.3. Major drivers of estuarine pCO₂ variability**

651

652 The pCO₂ in the surface mixed layer is a function of its temperature (T), salinity
653 (S_p), dissolved inorganic carbon (DIC) and total alkalinity (TAlk), as described by the
654 following relationship (Takahashi et al., 1993):

655

$$656 \quad dpCO_2 = (\partial pCO_2 / \partial T) dT + (\partial pCO_2 / \partial S_p) dS_p + (\partial pCO_2 / \partial DIC) dDIC + \\ 657 \quad (\partial pCO_2 / \partial TAlk) dTAlk \quad (9)$$

658

659 Through changes in T, S_p, DIC and TAlk, variations of surface-water pCO₂ are mainly
660 controlled by dynamic processes (water mass mixing), thermodynamic processes
661 (temperature and salinity changes), air-sea gas exchange, and biological processes
662 (photosynthesis, respiration) (Poisson et al., 1993). Among these, the effects of
663 temperature and DIC, i.e., the addition or removal of DIC through biological activity
664 and mixing processes, are generally the most important drivers of estuarine pCO₂
665 variability. In the absence of a significant source or sink of TAlk (e.g., calcium carbonate
666 formation/dissolution, anaerobic organic matter decomposition), changes of DIC
667 determine the buffer capacity (DIC/TAlk ratio) of the water. Whereas the physically and
668 biologically induced changes of DIC/pCO₂ will be quantified in a future study, using a
669 modified OMP water mass analysis, here, we evaluate the relative importance of
670 thermal and biological processes in controlling the spatial distribution of pCO₂ in the
671 St. Lawrence Estuary and Gulf.

672

673 To disentangle the biological and temperature effects on the spatial variability
674 of pCO₂, the DO(% sat) were plotted against the pCO₂(% sat), with the origin at 100 %
675 saturation for both gases. This simple approach uses the four possible combinations
676 of pCO₂(% sat)/DO(% sat) as integrated measures of thermally and biologically
677 induced changes. As shown in Fig. 8 (top), microbial respiration was the major driver
678 of pCO₂ variability in the USLE, whereas photosynthesis and temperature were the
679 dominant controls in the LSLE and GSL. We found similar results from a comparison of
680 eDIC and AOU (Fig. 8, bottom). In the strongly stratified Lower Estuary, as well as near

681 the estuary-gulf boundary, the biological drawdown of CO₂ counteracted the decrease
682 in CO₂ gas solubility due to increasing temperature (Fig. 9). Its waters were mostly
683 undersaturated with CO₂ with respect to the atmosphere (values of pCO₂ were below
684 atmospheric level) despite a general trend of surface-water warming (T = 2.7 to 12.6
685 °C). This pattern is consistent with the finding that, in spring/summer, the increasing
686 effect of warming on pCO₂ is counteracted by the photosynthetic utilization of CO₂,
687 particularly in a strongly stratified shallow mixed layer (Takahashi et al., 1993). Whereas
688 direct measurements of chlorophyll-a concentrations were not carried out during the
689 research cruises, a fluorescence sensor was mounted on the CTD probe. As shown in
690 Fig. 10, maximum fluorescence values, as well as high values of transmission (% light
691 transmission approaching 100%), were observed in the eastern Lower Estuary and the
692 western Gulf of St. Lawrence, where the system appears to shift from net heterotrophy
693 to net autotrophy. Farther into the Gulf (near Anticosti Island), the temperature
694 dependence of pCO₂ exerted a stronger influence, causing values of surface-water
695 pCO₂ to increase concomitantly with temperature (Fig. 9).

696

697 **4. Conclusions**

698

699 Because of its large physical dimensions and unimpeded connection to the
700 Atlantic Ocean, the St. Lawrence Estuary encompasses both a river-dominated inner
701 estuary, where physical mixing and abiotic processes dominate, and a marine-
702 dominated outer estuary, where biological cycling and oceanic processes prevail. The
703 physical and biogeochemical processes of these contrasting environments are
704 reflected in the spatial distribution of surface-water pCO₂ (139–765 μatm). The shallow,
705 partially mixed Upper Estuary, with a turbidity maximum controlled by tide- and wind-
706 induced turbulence, was, during our sampling period, a net source of CO₂ to the
707 atmosphere due to microbial respiration (low biological productivity), whereas the
708 deep, stratified Lower Estuary, with its stable, summertime three-layer vertical
709 structure, was generally a net sink of atmospheric CO₂ due to the enhanced biological
710 drawdown of pCO₂ (light availability, nutrient supply, strong stratification).

711

712 Overall, the large subarctic St. Lawrence Estuary was a weak source of CO₂ to
713 the atmosphere, with an area-averaged CO₂ degassing flux of 0.98 to 2.02 mmol C m⁻²
714 d⁻¹ (0.36 to 0.74 mol C m⁻² yr⁻¹). This efflux is somewhat smaller than the numerically

715 averaged CO₂ flux per unit area (2.19 mol C m⁻² yr⁻¹) reported from North American
716 estuaries by Chen et al. (2013), highlighting their relatively small contribution (~12 %)
717 to global estuarine CO₂ emissions. The pronounced shift in source/sink dynamics in
718 the St. Lawrence Estuary, between its river-dominated (9.2 ± 5.3 mmol m⁻² d⁻¹) and
719 marine-dominated (0.8 ± 7.2 mmol m⁻² d⁻¹) regions, is consistent with the conclusions
720 of the comparative study carried out by Jiang et al. (2008) that revealed large
721 differences in CO₂ degassing between riverine (inner) and maritime (outer) estuaries.
722 Given the limited research on CO₂ dynamics in large estuaries and bay systems, which
723 cover approximately one-half of the estuarine surface area on the U.S. east coast, as
724 well as the large uncertainties in the indirect measurement of pCO₂ (carbonic acid
725 dissociation constants, organic alkalinity contribution), current global-scale estimates
726 of estuarine CO₂ degassing may be overestimated. To better constrain the role of large
727 estuaries/bays in the coastal ocean carbon cycle, more extensive spatial and temporal
728 coverage of direct pCO₂ measurements across estuary types is needed.

729

730 **Data availability**

731 Data presented in this paper (Figures 4 and 8) are available upon request from one of the
732 authors (alfonso.mucci@mcgill.ca).

733

734 **Author contribution**

735 A.D. and A.M. conceived the project. A.M. acquired and processed the data prior to 2016. A.D.
736 conducted the data analysis and wrote the first draft of the paper whereas A.M. provided
737 editorial and scientific recommendations.

738

739 **Competing interests**

740 The authors declare that they have no conflict of interest.

741

742 **Acknowledgements**

743 We wish to thank the Captains and crews of the RV *Coriolis II* for their unwavering help over
744 the years. We also wish to acknowledge Gilles Desmeules and Michel Rousseau for their
745 dedicated electronic and field sampling support as well as Constance Guignard for her help in
746 cruise preparation and field data acquisition. Most of the data acquisition was carried out
747 opportunistically on research cruises funded by grants to A.M. or Canadian colleagues by the
748 Natural Sciences and Engineering Research Council of Canada (NSERC) whereas the work was
749 funded by a Regroupement Stratégique grant from the Fonds Québécois de Recherche Nature
750 et Technologies (FQRNT) to GEOTOP as well as NSERC Discovery and MEOPAR grants to A.M.

751 A.D. wishes to thank the Department of Earth and Planetary Sciences at McGill for financial
752 support in the form of scholarships and assistantships.

753

754 **References**

755

756 Abril, G., Etcheber, H., Borges, A. V., and Frankignoulle, M.: Excess atmospheric carbon
757 dioxide transported by rivers into the Scheldt estuary, *Cr. Acad. Sci. II A.*, 330, 761-768, 2000.

758

759 Abril, G., Commarieu, M. V., Sottolichio, A., Bretel, P., and Guerin, F.: Turbidity limits gas
760 exchange in a large macrotidal estuary, *Estuar. Coast. Shelf Sci.*, 83, 342-348, 2009.

761

762 Abril, G. et al.: Technical Note: Large overestimation of pCO₂ calculated from pH and alkalinity
763 in acidic, organic-rich freshwaters, *Biogeosciences*, 12, 67-78, 2015.

764

765 Bauer, J. E., Cai, W. J., Raymond, P. A., Bianchi, T. S., Hopkinson, C. S., and Regnier, P. A.: The
766 changing carbon cycle of the coastal ocean, *Nature*, 504, 61-70, 2013.

767

768 Benson, B. B. and Krause, D.: The concentration and isotopic fractionation of oxygen dissolved
769 in freshwater and seawater in equilibrium with the atmosphere, *Limnol. Oceanogr.*, 29, 620-
770 632, 1984.

771

772 Borges, A. V.: Do we have enough pieces of the jigsaw to integrate CO₂ fluxes in the coastal
773 ocean?, *Estuaries*, 28, 3-27, 2005.

774

775 Borges, A. V., and Abril, G.: Carbon dioxide and methane dynamics in estuaries, in: Wolanski,
776 E. and McLusky, D. S. (Eds.), *Treatise on Estuarine and Coastal Science*, Academic Press,
777 Waltham, 119-161, 2011.

778

779 Borges, A. V., Delille, B., Schiettecatte, L. S., Gazeau, F., Abril, G., and Frankignoulle, M.: Gas
780 transfer velocities of CO₂ in three European estuaries (Randers Fjord, Scheldt and Thames),
781 *Limnol. Oceanogr.*, 49, 1630-1641, 2004a.

782

783 Borges, A. V., Vanderborght, J. P., Schiettecatte, L. S., Gazeau, F., Ferrón-Smith, S., Delille, B.,
784 and Frankignoulle, M.: Variability of the gas transfer velocity of CO₂ in a macrotidal estuary (the
785 Scheldt), *Estuaries*, 27, 593-603, 2004b.

786

787 Borges, A. V., Delille, B., and Frankignoulle, M.: Budgeting sinks and sources of CO₂ in the
788 coastal ocean: Diversity of ecosystems counts, *Geophys. Res. Lett.*, 32, L14601,
789 doi:10.1029/2005GL023053, 2005.

790

791 Borges, A. V., Schiettecatte, L. S., Abril, G., Delille, B., and Gazeau, F.: Carbon dioxide in
792 European coastal waters, *Estuar. Coast. Shelf Sci.*, 70, 375-387, 2006.

793

794 Bugden, G. L.: Oceanographic conditions in the deeper waters of the Gulf of St. Lawrence in
795 relation to local and oceanic forcing, NAFO SCR document 88/87, 1988.

796

797 Byrne, R. H.: Standardization of standard buffers by visible spectrometry, *Anal. Chem.*, 59,
798 1479-1481, 1987.

799

800 Cai, W. J.: Estuarine and coastal ocean carbon paradox: CO₂ sinks or sites of terrestrial carbon
801 incineration?, *Annual Review of Marine Science*, 3, 123-145, 2011.

802

803 Cai, W. J. and Wang, Y.: The chemistry, fluxes, and sources of carbon dioxide in the estuarine
804 waters of the Satilla and Altamaha Rivers, Georgia, *Limnol. Oceanogr.*, 43, 657-668, 1998.

805

806 Carrillo, C. J., Smith, R. C., and Karl, D. M.: Processes regulating oxygen and carbon dioxide in
807 surface waters west of the Antarctic Peninsula, *Mar. Chem.*, 84, 161-179, 2004.

808

809 Cerco, C. F.: Estimating estuarine reaeration rates, *J. Environ. Eng.-ASCE*, 115, 1066-1070,
810 1989.

811

812 Chen, C. T. A. and Borges, A. V.: Reconciling opposing views on carbon cycling in the coastal
813 ocean: continental shelves as sinks and near-shore ecosystems as sources of atmospheric CO₂,
814 *Deep-Sea Res. Pt. II*, 56, 578-590, 2009.

815

816 Chen, C. T. A., Huang, T. H., Fu, Y. H., Bai, Y., and He, X.: Strong sources of CO₂ in upper
817 estuaries become sinks of CO₂ in large river plumes, *Current Opinion in Environmental*
818 *Sustainability*, 4, 179-185, 2012.

819

820 Chen, C. T. A., Huang, T. H., Chen, Y. C., Bai, Y., He, X., and Kang, Y.: Air-sea exchanges of CO₂
821 in the world's coastal seas, *Biogeosciences*, 10, 6509-6544, 2013.

822

823 Clayton, T. D. and Byrne, R. H.: Spectrophotometric seawater pH measurements: total
824 hydrogen ion concentration scale calibration of m-cresol purple and at-sea results, *Deep-Sea*
825 *Res. Pt. I*, 40, 2115-2129, 1993.

826

827 Cloern, J. E.: Our evolving conceptual model of the coastal eutrophication problem, *Mar. Ecol.-*
828 *Prog. Ser.*, 210, 223-253, 2001.

829

830 Coote, A. R. and Yeats, P. A.: Distribution of nutrients in the Gulf of St. Lawrence, *J. Fish. Res.*
831 *Board Can.*, 36, 122-131, 1979.

832

833 Cotovicz Jr., L. C., Knoppers, B. A., Brandini, N., Costa Santos, S. J., and Abril, G.: A strong CO₂
834 sink enhanced by eutrophication in a tropical coastal embayment (Guanabara Bay, Rio de
835 Janeiro, Brazil), *Biogeosciences*, 12, 6125-6146, 2015.

836

837 Cyr, F., Bourgault, D., Galbraith, P. S., and Gosselin, M.: Turbulent nitrate fluxes in the Lower St.
838 Lawrence Estuary, Canada, *J. Geophys. Res.-Oceans*, 120, 2308-2330, 2015.

839

840 d'Anglejan, B.: Recent sediments and sediment transport processes in the St. Lawrence
841 Estuary, in: El-Sabh, M. I. and Silverberg, N. (Eds.), *Oceanography of a Large-scale Estuarine*
842 *System*, Springer-Verlag, New York, 109-129, 1990.

843

844 d'Anglejan, B. F. and Smith, E. C.: Distribution, transport, and composition of suspended
845 matter in the St. Lawrence estuary, *Can. J. Earth Sci.*, 10, 1380-1396, 1973.

846

847 de Boyer Montégut, C., Madec, G., Fischer, A. S., Lazar, A., and Iudicone, D.: Mixed layer depth
848 over the global ocean: An examination of profile data and a profile-based climatology, *J.*
849 *Geophys. Res.*, 109, C12003, doi:10.1029/2004JC002378, 2004.

850

851 Dickson, A. G. and Goyet, C. (Eds.): *Handbook of Methods for the Analysis of the Various*
852 *Parameters of the Carbon Dioxide System in Sea Water (Version 2)*, U.S. Department of Energy,
853 ORNL/CDIAC-74, 1994.

854

855 Dickson, A. G., Sabine, C. L., and Christian, J. R. (Eds.): *Guide to Best Practices for Ocean CO₂*
856 *Measurements*, PICES Special Publication 3, 191 pp., 2007.

857

858 Dufour, R. and Ouellet, P.: Estuary and Gulf of St. Lawrence marine ecosystem overview and
859 assessment report, *Can. Tech. Rep. Fish. Aquat. Sci.*, 2744E, 112 pp., 2007.

860
861 El-Sabh, M. I. and Murty, T. S.: Mathematical modelling of tides in the St. Lawrence Estuary, in:
862 El-Sabh, M. I. and Silverberg, N. (Eds.), *Oceanography of a Large-scale Estuarine System*,
863 Springer-Verlag, New York, 10-50, 1990.
864
865 El-Sabh, M. I. and Silverberg, N.: The St. Lawrence Estuary: introduction, in: El-Sabh, M. I. and
866 Silverberg, N. (Eds.), *Oceanography of a Large-scale Estuarine System*, Springer-Verlag, New
867 York, 1-9, 1990.
868
869 Frankignoulle, M. et al.: Carbon dioxide emission from European estuaries, *Science*, 282, 434-
870 436, 1998.
871
872 Galbraith, P. S.: Winter water masses in the Gulf of St. Lawrence, *J. Geophys. Res.*, 111, C06022,
873 doi:10.1029/2005JC003159, 2006.
874
875 Gearing, J. N. and Pocklington, R.: Organic geochemical studies in the St. Lawrence Estuary,
876 in: El-Sabh, M. I. and Silverberg, N. (Eds.), *Oceanography of a Large-scale Estuarine System*,
877 Springer-Verlag, New York, 170-201, 1990.
878
879 Gilbert, D., Sundby, B., Gobeil, C., Mucci, A., and Tremblay, G. H.: A seventy-two-year record
880 of diminishing deep-water oxygen in the St. Lawrence estuary: The northwest Atlantic
881 connection, *Limnol. Oceanogr.*, 50, 1654-1666, 2005.
882
883 Grasshoff, K., Kremling, K., and Ehrhardt, M. (Eds.): *Methods of Seawater Analysis* (3rd ed.),
884 Wiley-VCH, Weinheim, Germany, 1999.
885
886 Gratton, Y., Mertz, G., and Gagné, J. A.: Satellite observations of tidal upwelling and mixing in
887 the St. Lawrence Estuary, *J. Geophys. Res.-Oceans*, 93, 6947-6954, 1988.
888
889 Hélie, J. F. and Hillaire-Marcel, C.: Sources of particulate and dissolved organic carbon in the
890 St Lawrence River: isotopic approach, *Hydrol. Process.*, 20, 1945-1959, 2006.
891
892 Hélie, J. F., Hillaire-Marcel, C., and Rondeau, B.: Seasonal changes in the sources and fluxes of
893 dissolved inorganic carbon through the St. Lawrence River—isotopic and chemical constraint,
894 *Chem. Geol.*, 186, 117-138, 2002.
895

896 Ho, D. T., Wanninkhof, R., Schlosser, P., Ullman, D. S., Hebert, D., and Sullivan, K. F.: Toward a
897 universal relationship between wind speed and gas exchange: Gas transfer velocities
898 measured with $3\text{He}/\text{SF}_6$ during the Southern Ocean Gas Exchange Experiment, *J. Geophys.*
899 *Res.*, 116, C00F04, doi:10.1029/2010JC006854, 2011.

900

901 Hunt, C. W., Salisbury, J. E., and Vandemark, D.: Contribution of non-carbonate anions to total
902 alkalinity and overestimation of pCO_2 in New England and New Brunswick rivers,
903 *Biogeosciences*, 8, 3069–3076, 2011.

904

905 Ingram, R. G. and El-Sabh, M. I.: Fronts and mesoscale features in the St. Lawrence Estuary, in:
906 El-Sabh, M. I. and Silverberg, N. (Eds.), *Oceanography of a Large-scale Estuarine System*,
907 Springer-Verlag, New York, 71–93, 1990.

908

909 Jiang, L. Q., Cai, W. J., and Wang, Y.: A comparative study of carbon dioxide degassing in river-
910 and marine-dominated estuaries, *Limnol. Oceanogr.*, 53, 2603–2615, 2008.

911

912 Joesoef, A., Huang, W. J., Gao, Y., and Cai, W. J.: Air-water fluxes and sources of carbon
913 dioxide in the Delaware Estuary: spatial and seasonal variability, *Biogeosciences*, 12, 6085-
914 6101, 2015.

915

916 Kaul, L. W. and Froelich, P. N.: Modeling estuarine nutrient geochemistry in a simple system,
917 *Geochim. Cosmochim. Acta*, 48, 1417–1433, 1984.

918

919 Koné, Y. J. M., Abril, G., Kouadio, K. N., Delille, B., and Borges, A. V.: Seasonal variability of
920 carbon dioxide in the rivers and lagoons of Ivory Coast (West Africa), *Estuaries and Coasts*, 32,
921 246–260, 2009.

922

923 Larouche, P., Koutitonsky, V. G., Chanut, J. P., and El-Sabh, M. I.: Lateral stratification and
924 dynamic balance at the Matane transect in the lower Saint Lawrence estuary, *Estuar. Coast.*
925 *Shelf Sci.*, 24, 859–871, 1987.

926

927 Laruelle, G. G., Dürr, H. H., Slomp, C. P., and Borges, A. V.: Evaluation of sinks and sources of
928 CO_2 in the global coastal ocean using a spatially-explicit typology of estuaries and continental
929 shelves, *Geophys. Res. Lett.*, 37, L15607, doi:10.1029/2010GL043691, 2010.

930

931 Laruelle, G. G., Dürr, H. H., Lauerwald, R., Hartmann, J., Slomp, C. P., Goossens, N., and Regnier,
932 P. A. G.: Global multi-scale segmentation of continental and coastal waters from the
933 watersheds to the continental margins, *Hydrol. Earth Syst. Sci.*, 17, 2029–2051, 2013.
934
935 Laruelle, G. G., Lauerwald, R., Rotschi, J., Raymond, P. A., Hartmann, J., and Regnier, P.:
936 Seasonal response of air-water CO₂ exchange along the land-ocean aquatic continuum of the
937 northeast North American coast, *Biogeosciences*, 12, 1447–1458, 2015.
938
939 Lucotte, M.: Organic carbon isotope ratios and implications for the maximum turbidity zone of
940 the St Lawrence upper estuary, *Estuar. Coast. Shelf Sci.*, 29, 293–304, 1989.
941
942 Lucotte, M. and d'Anglejan, B.: Seasonal control of the Saint-Lawrence maximum turbidity zone
943 by tidal-flat sedimentation, *Estuaries*, 9, 84–94, 1986.
944
945 Lucotte, M., Hillaire-Marcel, C., and Louchouart, P.: First-order organic carbon budget in the
946 St Lawrence Lower Estuary from ¹³C data, *Estuar. Coast. Shelf Sci.*, 32, 297–312, 1991.
947
948 Lueker, T. J., Dickson, A. G., and Keeling, C. D.: Ocean pCO₂ calculated from dissolved
949 inorganic carbon, alkalinity, and equations for K₁ and K₂: validation based on laboratory
950 measurements of CO₂ in gas and seawater at equilibrium, *Mar. Chem.*, 70, 105–119, 2000.
951
952 Maher, D. T., and Eyre, B. D.: Carbon budgets for three autotrophic Australian estuaries:
953 Implications for global estimates of the coastal air-water CO₂ flux, *Global Biogeochem. Cycles*,
954 26, GB1032, doi:10.1029/2011GB004075, 2012.
955
956 McDougall, T. J. and Barker, P. M.: Getting started with TEOS-10 and the Gibbs Seawater
957 (GSW) Oceanographic Toolbox, SCOR/IAPSO WG127, ISBN 978-0-646-55621-5, 28 pp., 2011.
958
959 Mertz, G. and Gratton, Y.: Topographic waves and topographically induced motions in the St.
960 Lawrence Estuary, in: El-Sabh, M. I. and Silverberg, N. (Eds.), *Oceanography of a Large-scale*
961 *Estuarine System*, Springer-Verlag, New York, 94–108, 1990.
962
963 Middelburg, J. J. and Herman, P. M.: Organic matter processing in tidal estuaries, *Mar. Chem.*,
964 106, 127–147, 2007.
965
966 Millero, F. J.: The thermodynamics of the carbonate system in seawater, *Geochim. Cosmochim.*
967 *Acta*, 43, 1651–1661, 1979.

968
969 Millero, F. J.: The pH of estuarine waters, *Limnol. Oceanogr.*, 31, 839-847, 1986.
970
971 Millero, F. J.: Carbonate constants for estuarine waters, *Mar. Freshwater Res.*, 61, 139-142,
972 2010.
973
974 Monbet, Y.: Control of phytoplankton biomass in estuaries: a comparative analysis of microtidal
975 and macrotidal estuaries, *Estuaries*, 15, 563-571, 1992.
976
977 Mucci, A., Levasseur, M., Gratton, Y., Martias, C., Scarratt, M., Gilbert, D., Tremblay, J.-É.,
978 Ferreya, G., and Lansard, B.: Tidal-induced variations of pH at the head of the Laurentian
979 Channel, *Can. J. Fish. Aquat. Sci.* (in revision), 2016.
980
981 Orr, J. C., Epitalon, J. M., and Gattuso, J. P.: Comparison of ten packages that compute ocean
982 carbonate chemistry, *Biogeosciences*, 12, 1483-1510, 2015.
983
984 Painchaud, J. and Therriault, J. C.: Relationships between bacteria, phytoplankton and
985 particulate organic carbon in the upper St. Lawrence estuary, *Mar. Ecol.-Prog. Ser.*, 56, 301-
986 311, 1989.
987
988 Painchaud, J., Lefavre, D., Therriault, J. C., and Legendre, L.: Physical processes controlling
989 bacterial distribution and variability in the upper St. Lawrence estuary, *Estuaries*, 18, 433-444,
990 1995.
991
992 Pelletier, E. and Lebel, J.: Hydrochemistry of dissolved inorganic carbon in the St. Lawrence
993 Estuary (Canada), *Estuar. Coast. Mar. Sci.*, 9, 785-795, 1979.
994
995 Peng, T. H., Takahashi, T., Broecker, W. S., and Olafsson, J.: Seasonal variability of carbon
996 dioxide, nutrients and oxygen in the northern North Atlantic surface water: observations and a
997 model, *Tellus*, 39B, 439-458, 1987.
998
999 Plourde, S. and Runge, J. A.: Reproduction of the planktonic copepod *Calanus finmarchicus* in
1000 the Lower St. Lawrence Estuary: relation to the cycle of phytoplankton production and
1001 evidence for a *Calanus* pump, *Mar. Ecol.-Prog. Ser.*, 102, 217-227, 1993.
1002
1003 Pocklington, R. and Leonard, J. D.: Terrigenous organic matter in sediments of the St. Lawrence
1004 Estuary and the Saguenay Fjord, *J. Fish. Res. Board Can.*, 36, 1250-1255, 1979.

1005
1006 Poisson, A., Metzl, N., Brunet, C., Schauer, B., Bres, B., Ruiz-Pino, D., and Louanchi, F.: Variability
1007 of sources and sinks of CO₂ in the Western Indian and Southern Oceans during the year 1991,
1008 J. Geophys. Res.-Oceans, 98, 22759-22778, 1993.
1009
1010 Raymond, P. A. and Cole, J. J.: Gas exchange in rivers and estuaries: Choosing a gas transfer
1011 velocity, Estuaries, 24, 312-317, 2001.
1012
1013 Raymond, P. A., Bauer, J. E., and Cole, J. J.: Atmospheric CO₂ evasion, dissolved inorganic
1014 carbon production, and net heterotrophy in the York River estuary, Limnol. Oceanogr., 45,
1015 1707-1717, 2000.
1016
1017 Regnier, P. et al.: Anthropogenic perturbation of the carbon fluxes from land to ocean, Nat.
1018 Geosci., 6, 597-607, 2013.
1019
1020 Richey, J. E., Devol, A. H., Wofsy, S. C., Victoria, R., and Riberio, M. N.: Biogenic gases and the
1021 oxidation and reduction of carbon in Amazon River and floodplain waters, Limnol. Oceanogr.,
1022 33, 551-561, 1988.
1023
1024 Robert-Baldo, G. L., Morris, M. J., and Byrne, R. H.: Spectrophotometric determination of
1025 seawater pH using phenol red, Anal. Chem., 57, 2564-2567, 1985.
1026
1027 Roy, R. N. et al.: The dissociation constants of carbonic acid in seawater at salinities 5 to 45 and
1028 temperatures 0 to 45°C, Mar. Chem., 44, 249-267, 1993.
1029
1030 Saucier, F. J. and Chassé, J.: Tidal circulation and buoyancy effects in the St. Lawrence Estuary,
1031 Atmos. Ocean, 38, 505-556, 2000.
1032
1033 Saucier, F. J., Roy, F., Gilbert, D., Pellerin, P., and Ritchie, H.: Modeling the formation and
1034 circulation processes of water masses and sea ice in the Gulf of St. Lawrence, Canada. J.
1035 Geophys. Res., 108, 3269, doi:10.1029/2000JC000686, 2003.
1036
1037 Savenkoff, C., Comeau, L., Vézina, A. F., and Gratton, Y.: Seasonal variation of the biological
1038 activity in the lower St. Lawrence Estuary, Can. Tech. Rep. Fish. Aquat. Sci., 2006, 22 pp., 1994.
1039
1040 Silverberg, N. and Sundby, B.: Observations in the turbidity maximum of the St. Lawrence
1041 estuary, Can. J. Earth Sci., 16, 939-950, 1979.

1042
1043 Sprintall, J. and Tomczak, M.: Evidence of the barrier layer in the surface layer of the tropics, J.
1044 Geophys. Res.-Oceans, 97, 7305-7316, 1992.
1045
1046 Statham, P. J.: Nutrients in estuaries—an overview and the potential impacts of climate change,
1047 Sci. Total Environ., 434, 213-227, 2012.
1048
1049 Takahashi, T., Olafsson, J., Goddard, J. G., Chipman, D. W., and Sutherland, S. C.: Seasonal
1050 variation of CO₂ and nutrients in the high-latitude surface oceans: a comparative study, Global
1051 Biogeochem. Cycles, 7, 843-878, 1993.
1052
1053 Takahashi, T. et al.: Global sea-air CO₂ flux based on climatological surface ocean pCO₂, and
1054 seasonal biological and temperature effects, Deep-Sea Res. Pt. II, 49, 1601-1622, 2002.
1055
1056 Tan, F. C. and Strain, P. M.: Sources, sinks and distribution of organic carbon in the St. Lawrence
1057 Estuary, Canada, Geochim. Cosmochim. Acta, 47, 125-132, 1983.
1058
1059 Tee, K-T.: Meteorologically and buoyancy induced subtidal salinity and velocity variations in
1060 the St. Lawrence Estuary, in: El-Sabh, M. I. and Silverberg, N. (Eds.), Oceanography of a Large-
1061 scale Estuarine System, Springer-Verlag, New York, 51-70, 1990.
1062
1063 Uncles, R. J., Stephens, J. A., and Smith, R. E.: The dependence of estuarine turbidity on tidal
1064 intrusion length, tidal range and residence time, Cont. Shelf Res., 22, 1835-1856, 2002.
1065
1066 van Heuven, S., Pierrot, D., Rae, J. W. B., Lewis, E., and Wallace, D. W. R.: MATLAB program
1067 developed for CO₂ system calculations, ORNL/CDIAC-105b, Carbon Dioxide Information
1068 Analysis Center, Oak Ridge National Laboratory, U.S. Department of Energy, Oak Ridge,
1069 Tennessee, doi: 10.3334/CDIAC/otg.CO2SYS_MATLAB_v1.1, 2011.
1070
1071 Wanninkhof, R.: Relationship between wind speed and gas exchange over the ocean, J.
1072 Geophys. Res.-Oceans, 97, 7373-7382, 1992.
1073
1074 Wanninkhof, R.: Relationship between wind speed and gas exchange over the ocean revisited,
1075 Limnol. Oceanogr.-Meth., 12, 351-362, 2014.
1076
1077 Weiss, R.: Carbon dioxide in water and seawater: the solubility of a non-ideal gas, Mar. Chem.,
1078 2, 203-215, 1974.

1079
1080 Weiss, R. F. and Price, B. A.: Nitrous oxide solubility in water and seawater, *Mar. Chem.*, 8, 347-
1081 359, 1980.
1082
1083 Working Group on the State of the St. Lawrence Monitoring, Overview of the State of the St.
1084 Lawrence 2014, St. Lawrence Action Plan, Environment Canada, Québec's ministère du
1085 Développement durable, de l'Environnement et de la Lutte contre les changements
1086 climatiques), Québec's ministère des Forêts, de la Faune et des Parcs, Parks Canada, Fisheries
1087 and Oceans Canada, and Stratégies Saint-Laurent, 52 pp., 2014.
1088
1089 Yang, B., Byrne, R. H., and Lindemuth, M.: Contributions of organic alkalinity to total alkalinity
1090 in coastal waters: A spectrophotometric approach, *Mar. Chem.*, 176, 199-207, 2015.
1091
1092 Yang, C., Telmer, K., and Veizer, J.: Chemical dynamics of the "St. Lawrence" riverine system:
1093 δD_{H_2O} , $\delta^{18}O_{H_2O}$, $\delta^{13}C_{DIC}$, $\delta^{34}S_{sulfate}$, and dissolved $^{87}Sr/^{86}Sr$, *Geochim. Cosmochim. Acta*, 60, 851-
1094 866, 1996.
1095
1096 Yeats, P. A.: Reactivity and transport of nutrients and metals in the St. Lawrence Estuary, in: El-
1097 Sabh, M. I. and Silverberg, N. (Eds.), *Oceanography of a Large-scale Estuarine System*,
1098 Springer-Verlag, New York, 155-169, 1990.
1099
1100 Zakardjian, B. A., Gratton, Y., and Vézina, A. F.: Late spring phytoplankton bloom in the Lower
1101 St. Lawrence Estuary: the flushing hypothesis revisited, *Mar. Ecol.-Prog. Ser.*, 192, 31-48, 2000.
1102
1103 Zappa, C. J., Raymond, P. A., Terray, E. A., and McGillis, W. R.: Variation in surface turbulence
1104 and the gas transfer velocity over a tidal cycle in a macro-tidal estuary, *Estuaries*, 26, 1401-
1105 1415, 2003.
1106
1107 Zappa, C. J., McGillis, W. R., Raymond, P. A., Edson, J. B., Hints, E. J., Zemmelen, H. J., Dacey,
1108 J. W. H., and Ho, D. T.: Environmental turbulent mixing controls on air-water gas exchange in
1109 marine and aquatic systems, *Geophys. Res. Lett.*, 34, L10601, doi:10.1029/2006GL028790,
1110 2007.
1111
1112
1113
1114
1115

1116 **Table 1.** Mean, standard deviation and range of the surface-water temperature (T),
 1117 practical salinity (S_p), dissolved inorganic carbon (DIC), total alkalinity (TAlk) and *in situ*
 1118 partial pressure of CO_2 (pCO_2) in the St. Lawrence River (near Québec City), Upper
 1119 Estuary (Île d'Orléans to Tadoussac), Lower Estuary (Tadoussac to Pointe-des-Monts)
 1120 and Gulf (Pointe-des-Monts to Cabot Strait) during all sampling months. Numbers in
 1121 parentheses indicate the ranges observed.

	T (°C)	S_p	DIC ($\mu\text{mol kg}^{-1}$)	TAlk ($\mu\text{mol kg}^{-1}$)	pCO_2 (μatm)
River (N=3)	14.2 ± 3.9 (9.8-17.2)	0.03 ± 0.05 (0-0.09)	1242 ± 132 (1148-1335)	1204 ± 99 (1124-1314)	604 ± 76 (550-658)
Upper (N=46)	9.6 ± 3.6 (4.2-17.4)	10.9 ± 8.0 (0-24.5)	1514 ± 242 (1081-2005)	1492 ± 272 (969-2030)	571 ± 72 (435-765)
Lower (N=60)	6.2 ± 2.2 (2.7-12.6)	26.2 ± 2.1 (21.2-30.4)	1837 ± 82 (1634-2005)	1957 ± 82 (1752-2088)	394 ± 119 (139-578)
Gulf (N=30)	8.8 ± 3.1 (3.9-13.7)	30.1 ± 1.5 (25.5-31.5)	1936 ± 64 (1761-2032)	2096 ± 61 (1921-2175)	352 ± 80 (207-478)

1122
 1123
 1124
 1125
 1126
 1127
 1128
 1129
 1130
 1131
 1132
 1133
 1134
 1135
 1136
 1137
 1138
 1139
 1140

1141 **Table 2.** Mean, standard deviation and range of $\Delta p\text{CO}_2$, k_{W-14} , $k_{R\&C-01}$, F_{W-14} and $F_{R\&C-01}$
 1142 in the surface waters of the St. Lawrence River, Upper Estuary, Lower Estuary and Gulf
 1143 during all sampling months. k_{W-14} are the gas transfer velocities given by the
 1144 Wanninkhof (2014) relationship, whereas $k_{R\&C-01}$ are those given by Raymond and Cole
 1145 (2001). Values of F_{W-14} are taken to be the theoretical lower limit of air-sea gas
 1146 exchange, whereas values of $F_{R\&C-01}$ are the upper limit. Numbers in parentheses
 1147 indicate the ranges observed; the extreme F data points are shown in bold.

	$\Delta p\text{CO}_2$ (μatm)	k_{W-14} (cm h^{-1})	$k_{R\&C-01}$ (cm h^{-1})	F_{W-14} ($\text{mmol m}^{-2} \text{d}^{-1}$)	$F_{R\&C-01}$ ($\text{mmol m}^{-2} \text{d}^{-1}$)
River (N=3)	217 ± 99 (147/287)	3.0 ± 1.4 (1.9/4.5)	6.1 ± 2.0 (4.3/8.2)	5.8 ± 3.2 (3.5/8.0)	12.7 ± 6.4 (8.2/ 17.3)
Upper (N=46)	184 ± 72 (43/386)	2.8 ± 0.8 (1.6/4.5)	5.6 ± 1.1 (3.8/8.1)	6.1 ± 3.0 (2.0/14.7)	12.3 ± 5.4 (3.6/ 28.4)
Lower (N=60)	9.2 ± 116 (-266/188)	3.2 ± 0.4 (2.0/3.8)	5.9 ± 0.6 (4.3/6.9)	0.6 ± 4.9 (-12.1/8.3)	1.0 ± 9.0 (-21.9/15.1)
Gulf (N=30)	-31.0 ± 90 (-178/107)	1.2 ± 0.3 (0.8/1.7)	3.4 ± 0.3 (2.8/4.1)	-0.8 ± 1.5 (-3.6/1.1)	-1.7 ± 3.9 (-8.4/3.6)

1148
 1149
 1150
 1151
 1152
 1153
 1154
 1155
 1156
 1157
 1158
 1159
 1160
 1161
 1162
 1163

1164 **Table 3.** Sectional and area-averaged air-sea CO₂ fluxes (mmol C m⁻² d⁻¹) in the St.
 1165 Lawrence Estuary during all sampling months. To obtain the area-averaged CO₂ flux,
 1166 the SLE was divided into five segments at equal intervals. The first row of the table
 1167 shows the surface area (km²) of each segment. The flux data in each segment were
 1168 numerically averaged to obtain sectional fluxes, which were then area weighted and
 1169 summed to obtain the spatially integrated whole-estuary flux (in bold). The F_{W-14} and
 1170 F_{R&C-01} data provide the lower and upper estimates, respectively.

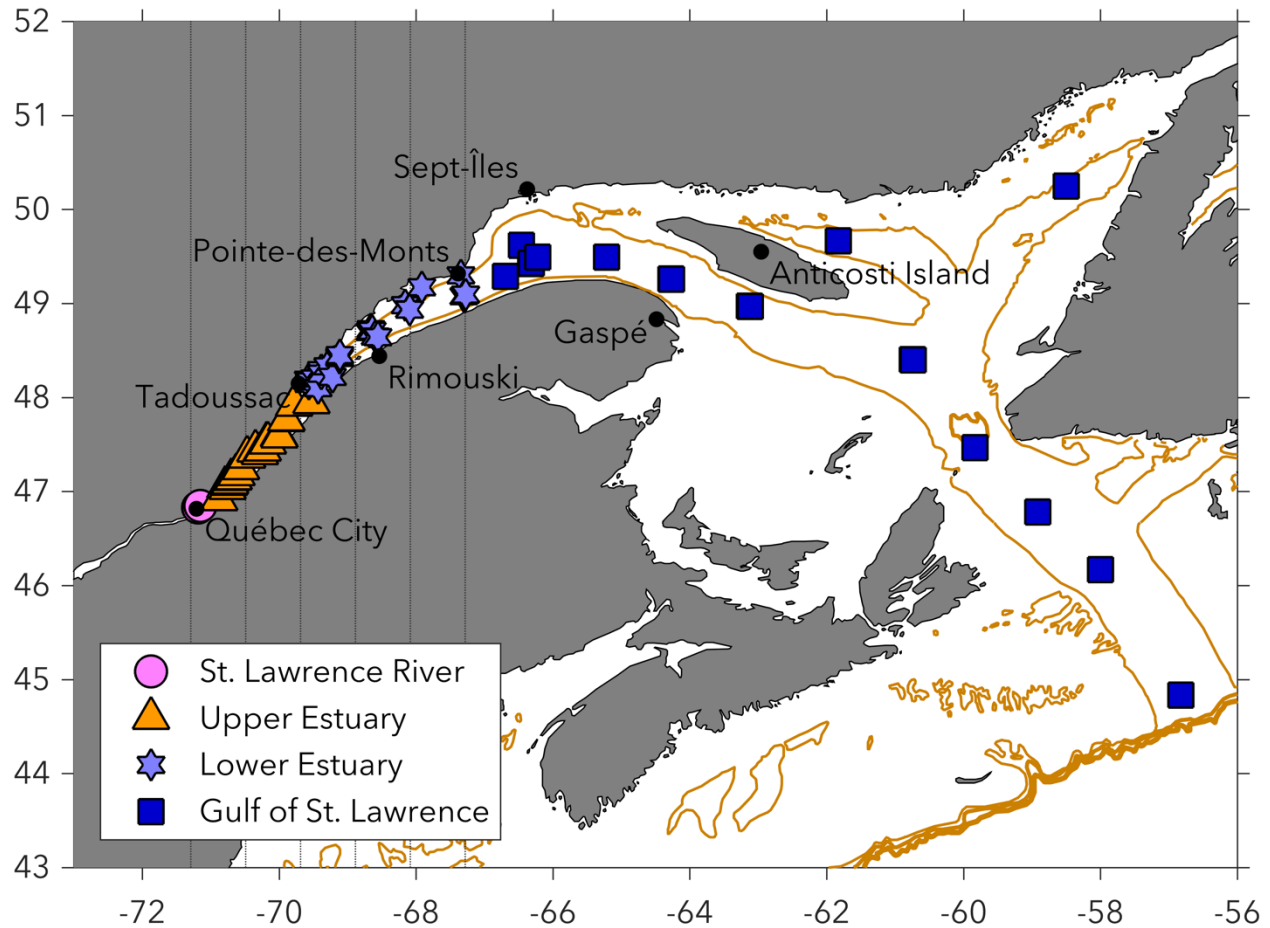
	Seg 1 (N=17)	Seg 2 (N=23)	Seg 3 (N=21)	Seg 4 (N=17)	Seg 5 (N=8)	Whole estuary
Surface area (km ²)	1,098	2,250	2,726	3,404	3,303	12,781
F _{W-14} (mmol m ⁻² d ⁻¹)	7.2	5.4	4.3	-1.8	-4.0	0.98
F _{R&C-01} (mmol m ⁻² d ⁻¹)	14.5	11.0	7.9	-3.5	-7.4	2.02

1171
 1172
 1173
 1174
 1175
 1176
 1177
 1178
 1179
 1180
 1181
 1182
 1183
 1184
 1185
 1186
 1187
 1188
 1189
 1190
 1191
 1192
 1193



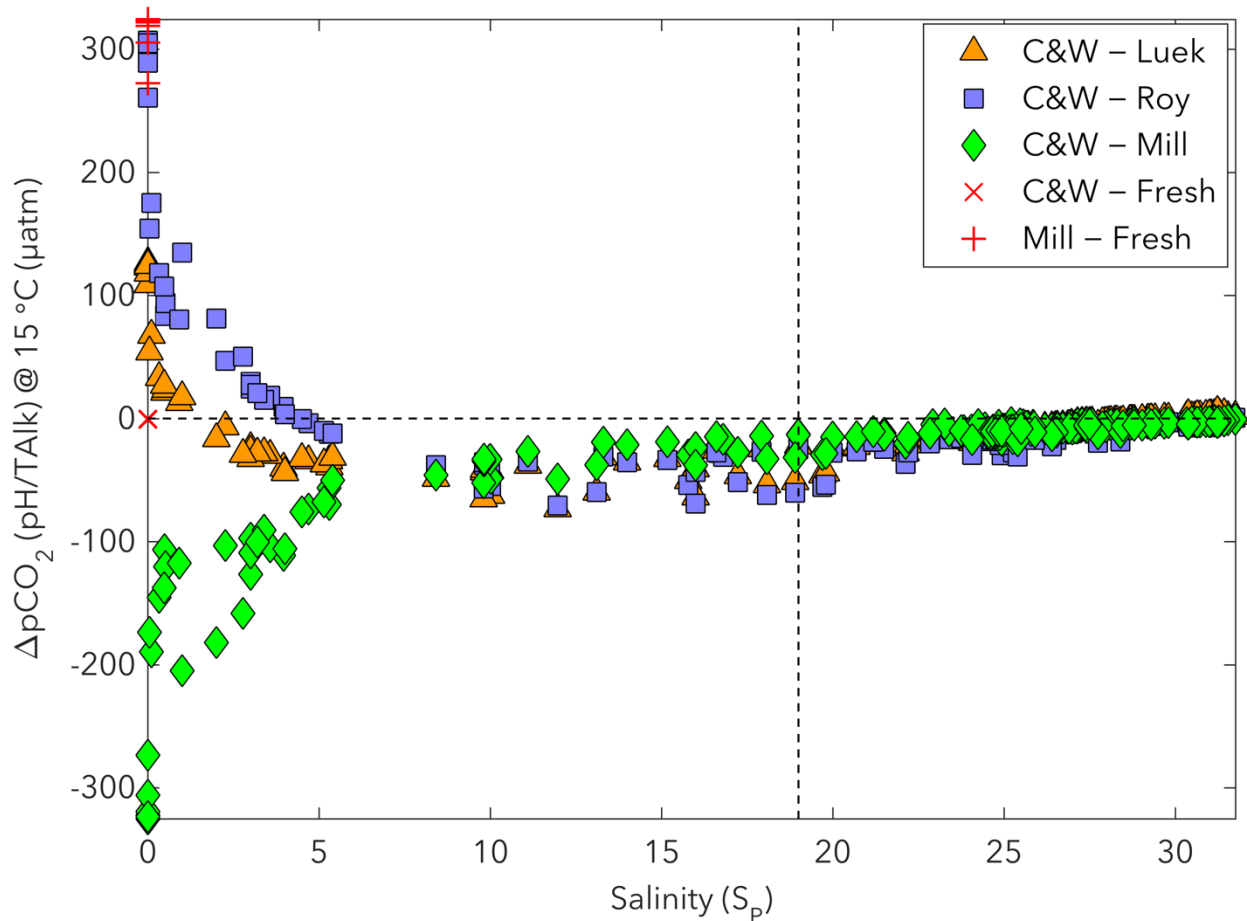
1194
 1195 **Figure 1.** Map of the greater St. Lawrence system, including the chain of Great Lakes,
 1196 the St. Lawrence River, the Upper St. Lawrence Estuary (USLE), the Lower St. Lawrence
 1197 Estuary (LSLE), and the Gulf of St. Lawrence (GSL). From: Overview of the State of the
 1198 St. Lawrence 2014 (with permission).

1199
 1200
 1201
 1202
 1203
 1204
 1205
 1206
 1207
 1208
 1209
 1210
 1211
 1212
 1213



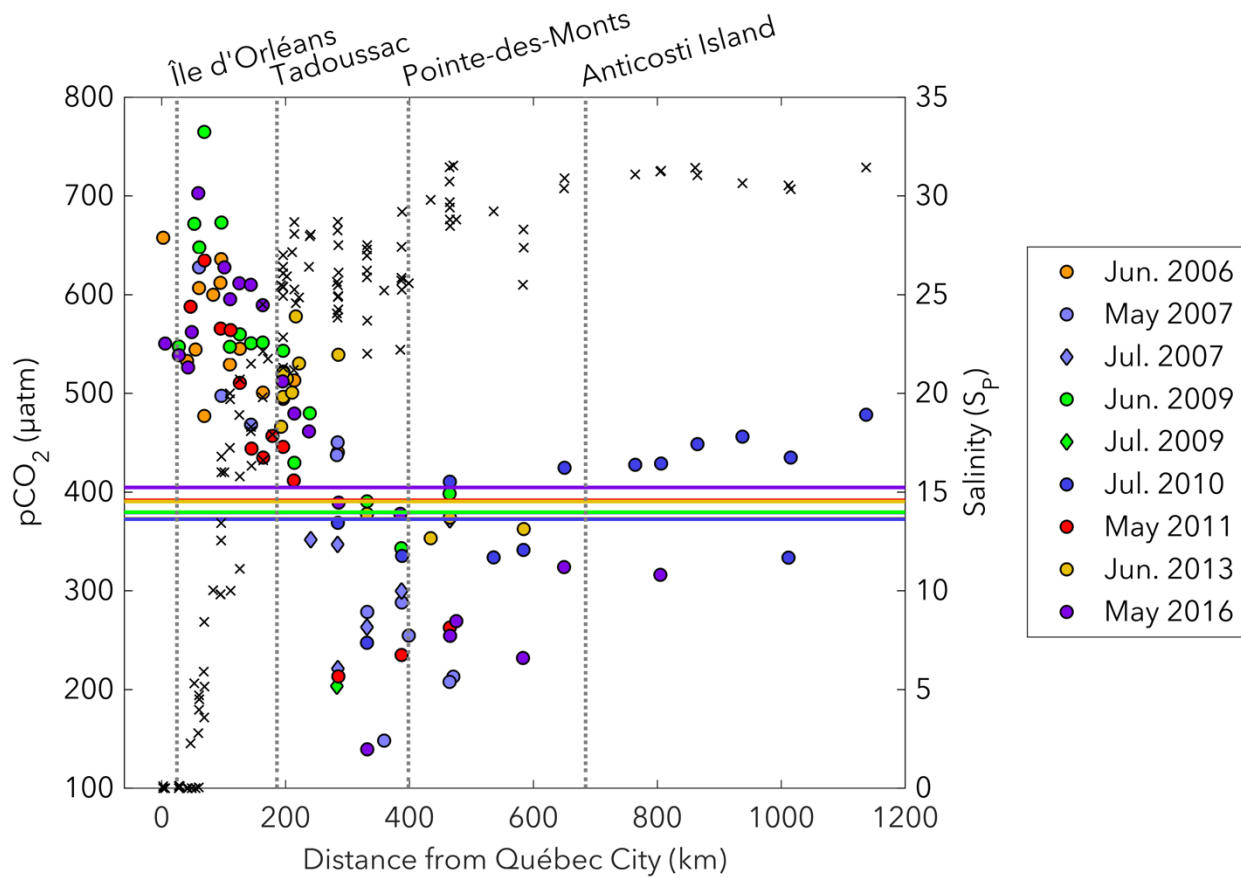
1214
 1215 **Figure 2.** Map showing the four principal subdivisions of the study area and the
 1216 sampling locations (markers). Water samples were collected during ten
 1217 spring/summer research cruises: July 2003, June 2006, May 2007, July 2007, June
 1218 2009, July 2009, July 2010, May 2011, June 2013 and May 2016. The estuary, from the
 1219 landward limit of the salt water intrusion near Île d'Orléans (~5 km downstream of
 1220 Québec City) to Pointe-des-Monts, where the coastline diverges, extends ~400 km and
 1221 covers a total surface area of ~12,820 km². The solid gold line follows the 200m isobath
 1222 of the Laurentian Channel. The vertical dotted lines delineate the five segments of the
 1223 estuary used for the calculation of the area-averaged CO₂ flux.

1224
 1225
 1226
 1227
 1228
 1229



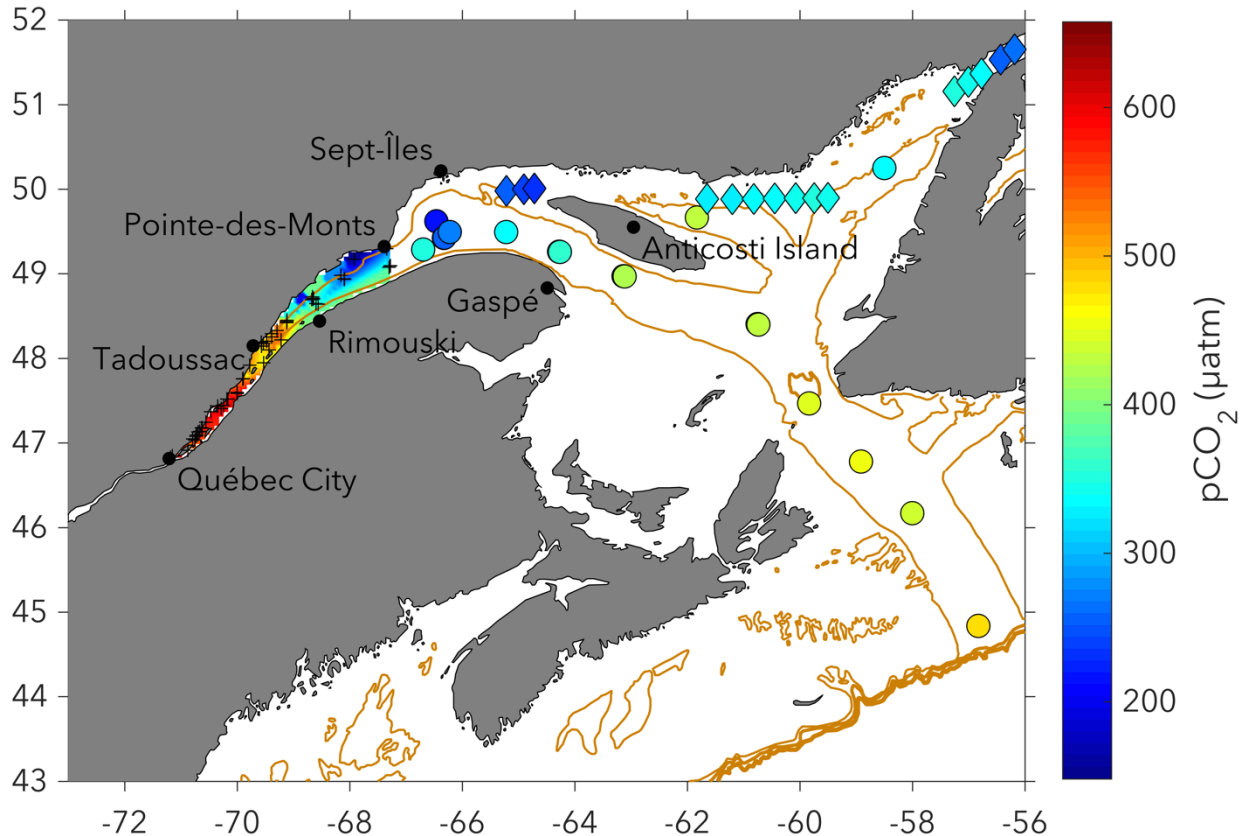
1230
 1231 **Figure 3.** Differences in $p\text{CO}_2$ ($\Delta p\text{CO}_2$) calculated using different published
 1232 formulations of K_1 and K_2 , including Cai and Wang (1998) [C&W], Lueker et al. (2000)
 1233 [Luek], Roy et al. (1993) [Roy], Millero (2010) [Mill], and Millero (1979) for pure water
 1234 only ($S_p = 0$) [Fresh]. All calculations were carried out at 15 °C ($p\text{CO}_2$ @ 15 °C) with
 1235 measured pH and TAlk. The constants of Lueker et al. (2000) are recommended for
 1236 best practices by Dickson et al. (2007) and are applicable for waters at $S_p > 19$
 1237 (delineated by the vertical dashed line), whereas those of Roy et al. (1993) ($S_p = 5$ to
 1238 45) are recommended by Dickson and Goyet (1994). Both the constants of Cai and
 1239 Wang (1998) and Millero (2010) have been proposed as more appropriate for the
 1240 study of the carbonate system in estuarine waters.

1241
 1242
 1243
 1244
 1245



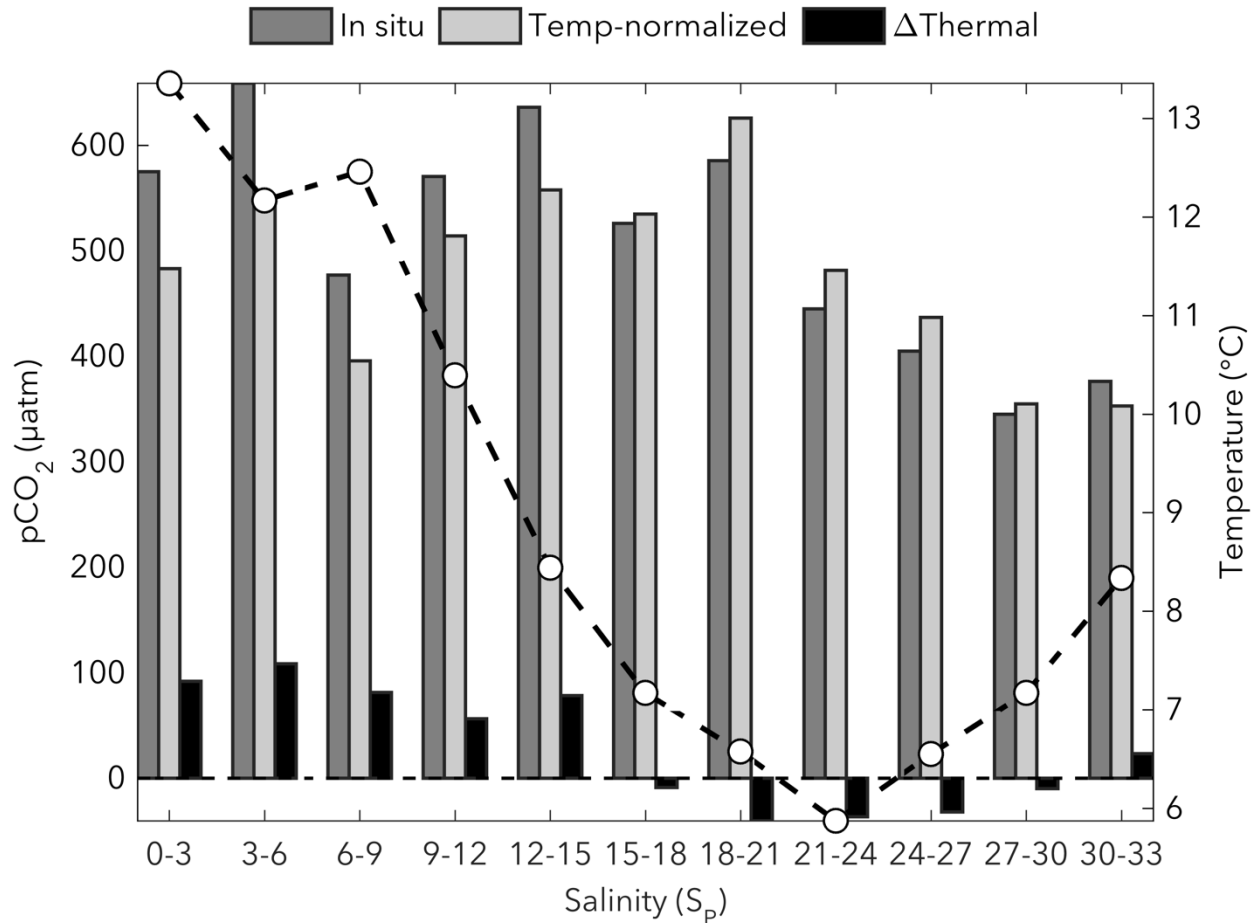
1246
 1247 **Figure 4.** Spatial distributions of surface-water pCO₂ (circles, diamonds) and practical
 1248 salinity (x symbols) in the St. Lawrence River, Estuary and Gulf during spring/summer
 1249 cruises. Horizontal lines show the mean pCO₂(air) in the sampling months. The pCO₂
 1250 data points above atmospheric level are sources of CO₂ to the atmosphere whereas
 1251 those below atmospheric level are sinks of atmospheric CO₂.

1252
 1253
 1254
 1255
 1256
 1257
 1258
 1259
 1260
 1261
 1262



1263
 1264 **Figure 5.** Spatial distribution of surface-water pCO₂ (µatm) in the St. Lawrence Estuary and Gulf during all spring/summer cruises. Linear interpolation was used between the
 1265 and Gulf during all spring/summer cruises. Linear interpolation was used between the
 1266 sampling locations in the estuary (+ symbols). Circles show calculated pCO₂ (pH/TALK),
 1267 whereas diamonds show pCO₂ measured by the underway system (General Oceanics
 1268 model 8050) aboard the CCGS *Amundsen* in June 2016 (Dr. Tim
 1269 Papakyriakou/University of Manitoba, pers. comm.). For neighboring locations
 1270 sampled in May 2016 aboard the RV *Coriolis II*, measured and calculated pCO₂ differed
 1271 by, on average, ~4.2 %. The mean atmospheric pCO₂ during the sampling months
 1272 ranged from 372 to 405 µatm.

1273
 1274
 1275
 1276
 1277
 1278
 1279
 1280



1281

1282 **Figure 6.** Surface-water *in situ* pCO_2 , temperature-normalized pCO_2 , and
 1283 $\Delta pCO_2(temp)$ averaged over salinity bins of 3. The open circles show the average
 1284 temperature for each salinity bin. To correct for the increasing/decreasing effect of
 1285 temperature on surface-water pCO_2 , the *in situ* pCO_2 were normalized to the average
 1286 surface-water temperature of the study area ($T = 7.82^{\circ}C$). The $\Delta pCO_2(temp)$ are the
 1287 thermally-induced pCO_2 changes due to temperature deviations from $T = 7.82^{\circ}C$,
 1288 whereas variations in temperature-normalized pCO_2 are due to water mass mixing
 1289 and/or biological activity.

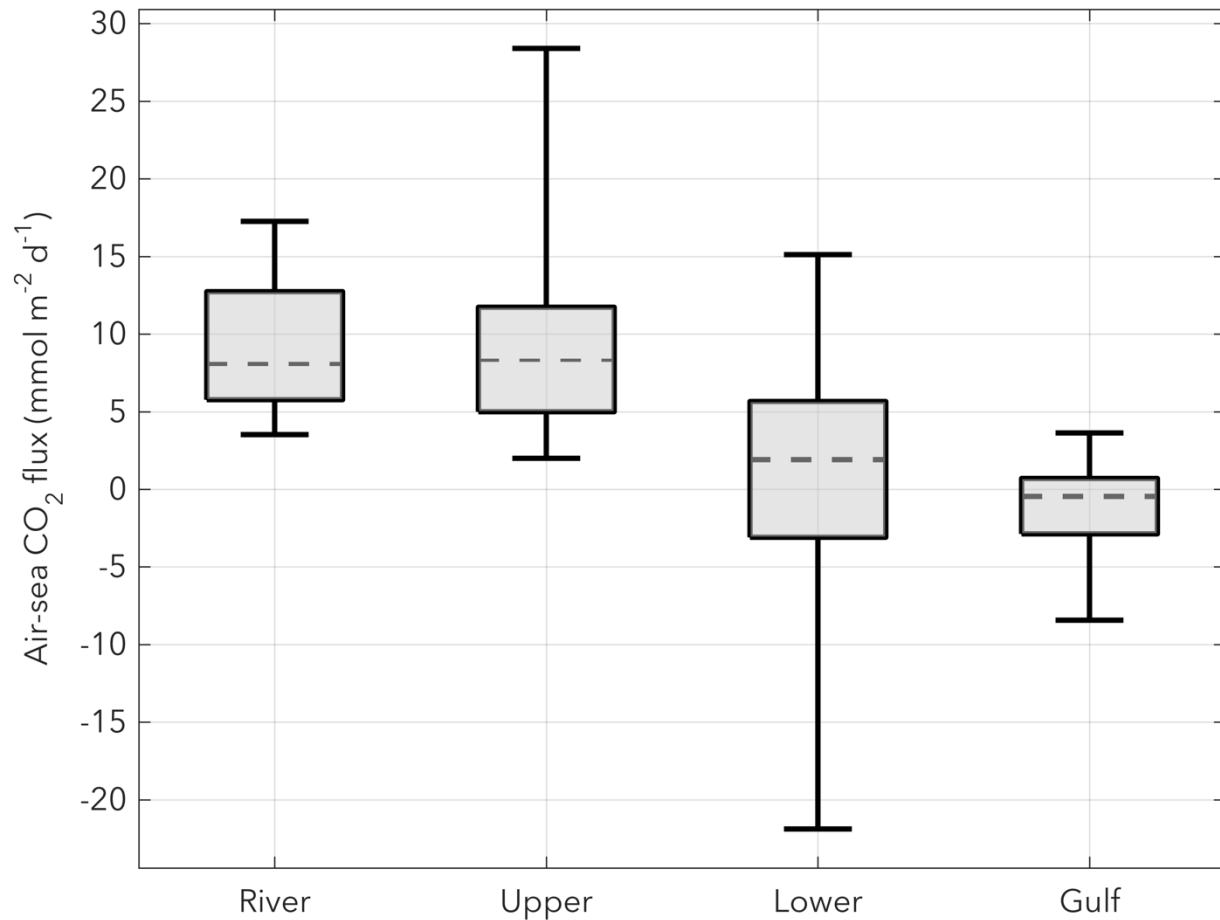
1290

1291

1292

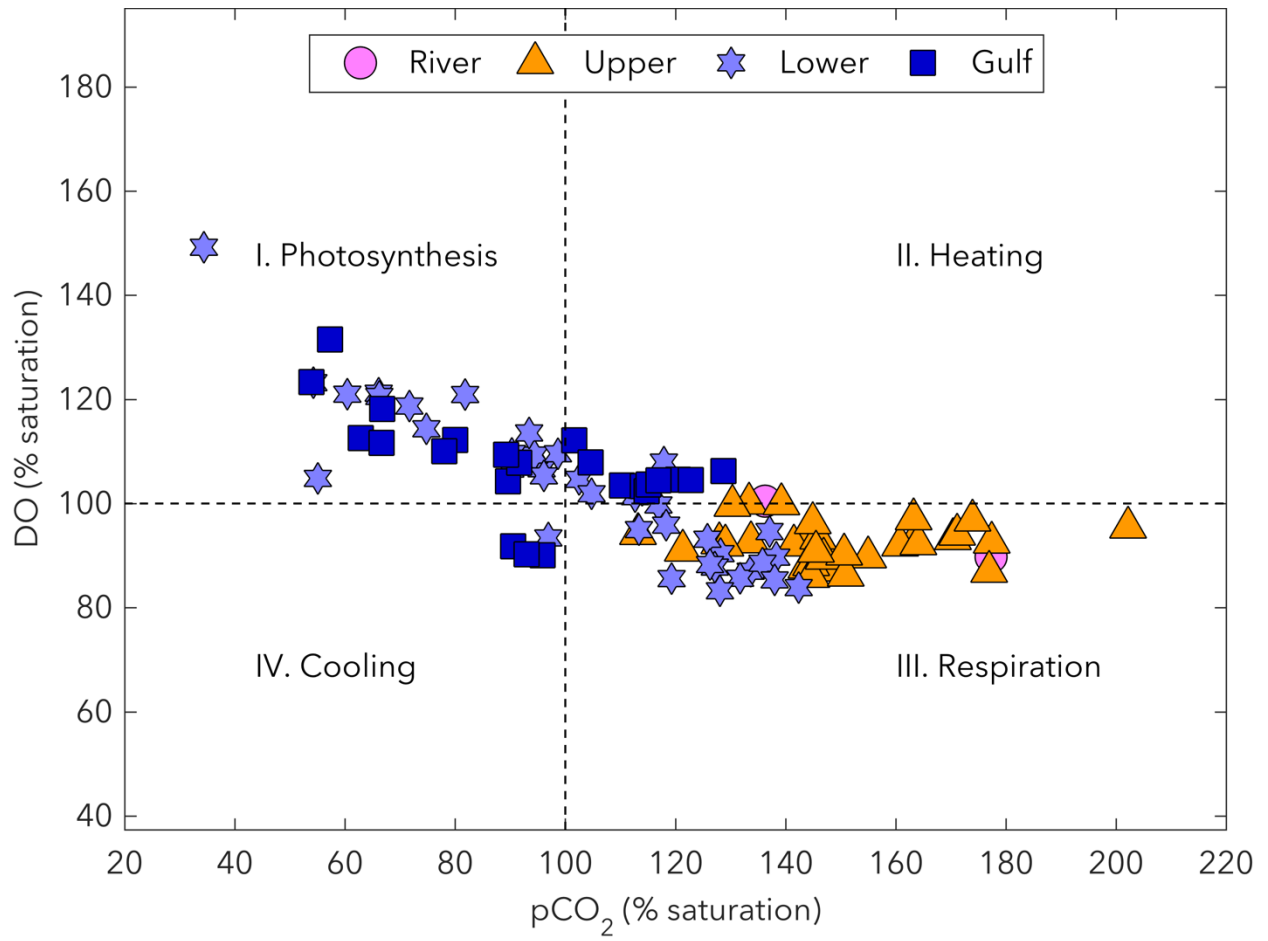
1293

1294

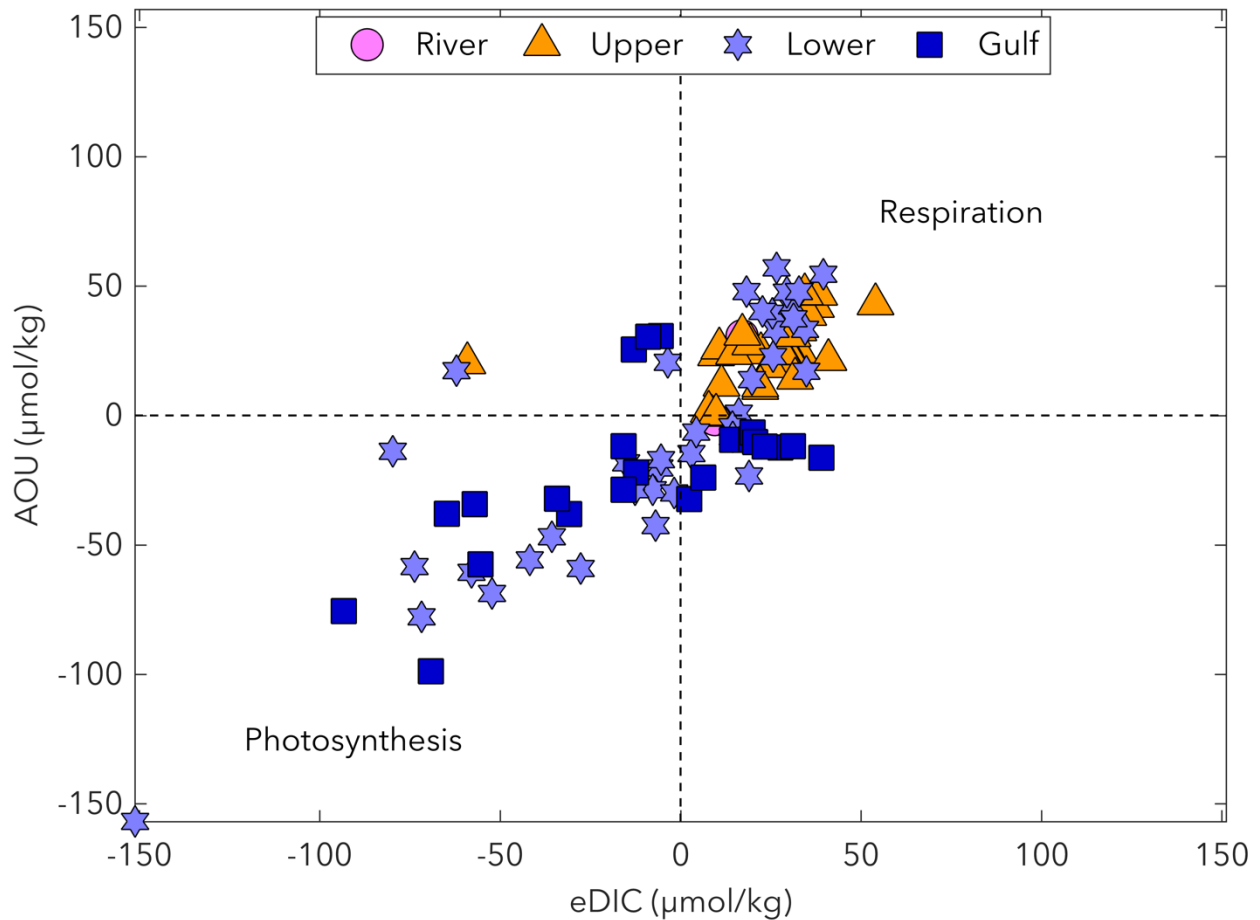


1295
 1296 **Figure 7.** Box plot showing the variability of air-sea CO₂ fluxes in the four principal
 1297 subdivisions of the study area (St. Lawrence River, Upper Estuary, Lower Estuary and
 1298 Gulf). The box spans the interquartile range (25-75 percentiles), the dashed line is the
 1299 median, and the whiskers extend to the extreme data points. The F_{W-14} data were
 1300 combined with the F_{R&C-01} data from all spring/summer sampling months to depict the
 1301 upper and lower limits of gas exchange.

1302
 1303
 1304
 1305
 1306
 1307
 1308



1309



1310

1311 **Figure 8.** Top: comparison of the saturation states (or % saturation) of pCO₂ and DO in
 1312 the mixed-layer waters of the St. Lawrence River, Estuary and Gulf. Dashed lines
 1313 delineate the 100 % saturation levels for both gases. Surface-water samples (markers)
 1314 fall into one of four quadrants representing the dominant controls on CO₂/O₂
 1315 dynamics. Quadrants I and III indicate the effects of photosynthesis/respiration,
 1316 whereas Quadrants II and IV indicate heating/cooling. Bottom: comparison of the
 1317 apparent oxygen utilization (AOU) and excess DIC (eDIC). Respiration/remineralization
 1318 processes are reflected in positive values of AOU and eDIC, whereas the effects of
 1319 photosynthesis are reflected in negative values.

1320

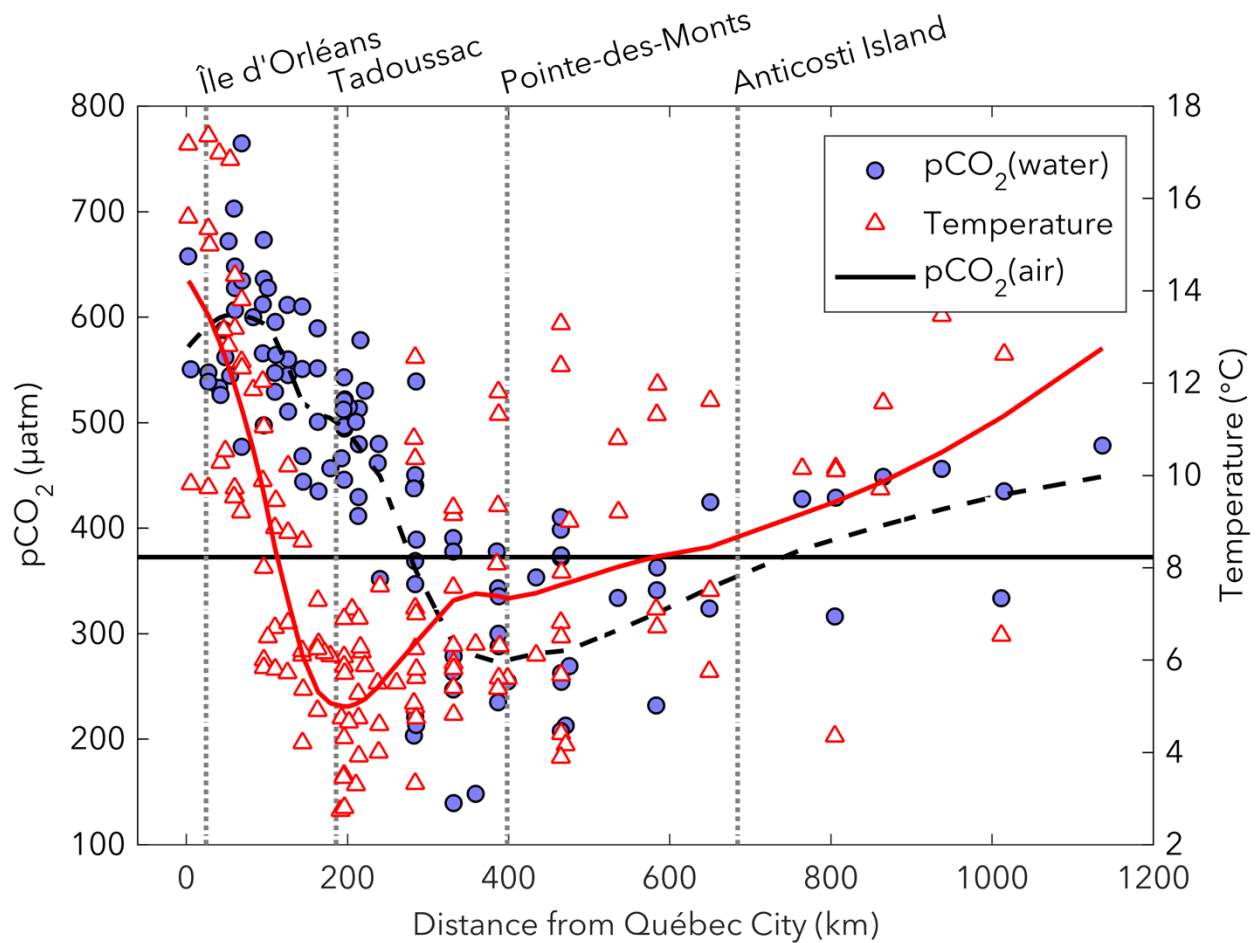
1321

1322

1323

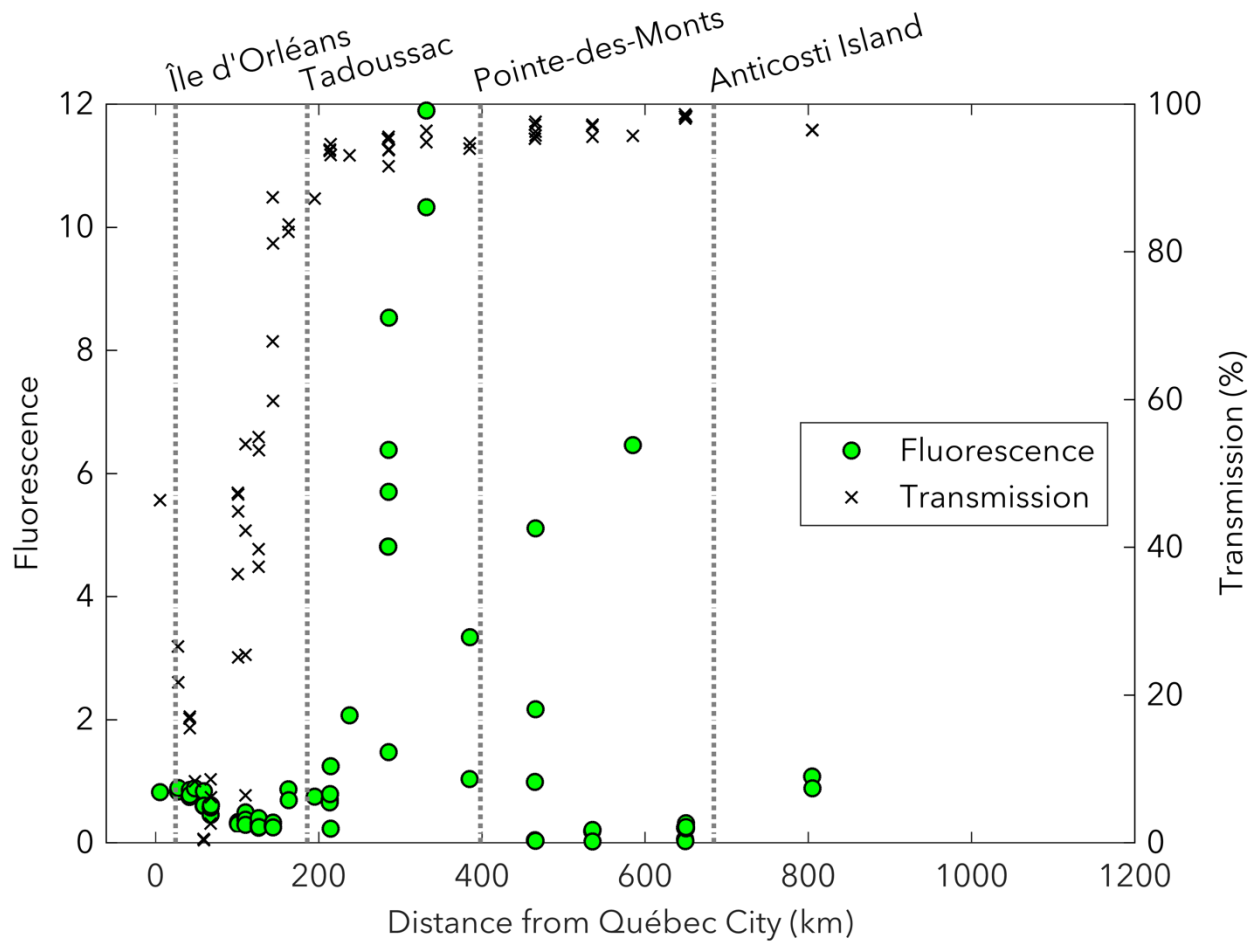
1324

1325



1326
 1327 **Figure 9.** Spatial distributions of surface-water pCO₂ (circles) and temperature
 1328 (triangles) in the St. Lawrence River, Estuary and Gulf during spring/summer cruises.
 1329 Temperatures ranged from 4.2 to 17.4 °C (generally decreasing) in the USLE, 2.7 to
 1330 12.6 °C (generally increasing) in the LSLE, and 3.9 to 13.7 °C (generally increasing) in
 1331 the GSL. The horizontal line shows the mean atmospheric pCO₂, pCO₂(air), during all
 1332 sampling months. The dashed line is the smoothed pCO₂(water) data using a moving
 1333 average filter with a span of 50% of the total number of data points, whereas the red
 1334 line is the smoothed temperature data.

1335
 1336
 1337
 1338
 1339
 1340
 1341



1342

1343 **Figure 10.** Spatial distributions of maximum fluorescence values (circles) and mean
 1344 transmission values (x symbols) in the euphotic zone of the St. Lawrence River, Estuary
 1345 and Gulf during the May 2016 cruise. Fluorescence is a primary production proxy,
 1346 whereas transmission is an excellent proxy for turbidity (low transmission values are
 1347 due to light absorption by suspended particulate matter and/or colored dissolved
 1348 organic matter).